UNITED STATES ATOMIC ENERGY COMMISSION

NYO-637

GAMMA-TRANSMISSION IN IRON, TUNGSTEN, LEAD, URANIUM, AND A PURE COMPTON SCATTERED BY ROOT-MEAN-SQUARE ANGLE CALCULATION

By
Leonard R. Solon
J. Ernest Wilkins, Jr.
Alan Oppenheim
Herbert Goldstein

April 5, 1951

Nuclear Development Associates, Inc.

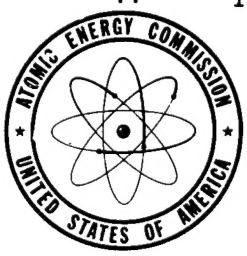

Technical Information Service, Oak Ridge, Tennessee

ABSTRACT

The root-mean-square angle technique reported earlier (NYO-635) is extended to the calculation of buildup factors in iron, tungsten, lead, and uranium for 1,..., 8 Mev photons and a pure Compton scatterer for 1, 2.5, and 10 mc^2 photons. Computations are carried out to 20 mean free paths for the metals and 40 mean free paths for the Compton scatterer. The behavior of the buildup factors as functions of the initial energy for the heavy elements is found to differ qualitatively from that for iron and the pure Compton scatterer.

PHYSICS

Reproduced direct from copy
as submitted to this office.

Work performed under
Contract No. AT(30-1)-862

PRINTED IN USA
PRICE 25 CENTS

AEC, Oak Ridge, Tenn., 5-29-51--925-W3982

Contents

GAMMA-TRANSMISSION IN IRON, TUNGSTEN, LEAD, URANIUM, AND A PURE COMPTON SCATTERER BY ROOT-MEAN-SQUARE ANGLE CALCULATION

by

Leonard R. Solon, J. Ernest Wilkins, Jr.,
Alan Oppenheim, Herbert Goldstein

Introduction

If the interactions of photons with matter were pure absorption processes the attenuation of gamma rays through a material could be simply calculated on the basis of an exponential decrease. Thus for a plane monodirectional and monoenergetic source the fraction, f, of photon flux surviving a penetration x would be merely

$$f = e^{-\mu_o x} . \qquad (1)$$

Here μ_o is the total macroscopic cross section of the photons for the given initial energy E_o.

In the Compton process, however, the photons are not absorbed, but merely degraded in energy and scattered from the incident direction. These secondary photons must be included in the calculation of the photon flux, and Eq. (1) for f must be replaced by

$$f = \left[1 + B(E_o, \mu_o x)\right] e^{-\mu_o x} . \qquad (2)$$

The quantity B is called the "buildup factor" and is the ratio of the secondary, scattered flux to the primary, unscattered flux. If f refers to the particle flux then the corresponding buildup factor is B_N, the "number buildup factor". If it is the energy flux, or intensity, that is involved, then the corresponding B is B_E, the "energy buildup factor".

Because of the difficulty in obtaining a rigorous solution to the transport equation describing the secondary photon spectrum, several approximate methods have been developed. One which has received considerable attention describes the energy degradation as correctly as possible, but assumes the photons are not deviated in direction by the Compton scattering. This "straight-ahead" approximation has been treated in considerable detail in Reference (1) and elsewhere. The so-called "R.M.S." method represents an attempt to improve the straight-ahead approximation by including, in some measure, the effect of angular deviations. Briefly, the method assumes that all photons of wavelength λ are traveling at a single angle Θ to the forward x direction given by the root-mean-square angle deviation corresponding to λ. Details of the method are described in References (2) and (10). The transport equation takes the form

$$\frac{\partial F(x,\lambda)}{\partial x} + \frac{\mu(\lambda)}{1-(\lambda-\lambda_o)} F(x,\lambda) = \int_{\lambda_o}^{\lambda} \frac{K(\lambda',\lambda)F(x,\lambda')}{1-(\lambda'-\lambda_o)} d\lambda' + K(\lambda_o,\lambda)e^{-\mu_o x} \qquad (3)$$

where the symbols have the following meanings:

$F(x,\lambda)d\lambda$ is the particle flux of secondary photons at distance x with wavelength in units of the Compton wavelength between λ and $\lambda+d\lambda$,

λ_o is the wavelength corresponding to the initial energy,

$\mu(\lambda)$ is the total macroscopic absorption coefficient, and

$$K(\lambda',\lambda) = A\left(\frac{\lambda'}{\lambda}\right)^2\left[\frac{\lambda}{\lambda'} + \frac{\lambda'}{\lambda} - (\lambda-\lambda')\left\{2-(\lambda-\lambda')\right\}\right] \qquad (4)$$

where A is a constant depending on the electron density of the medium. In terms of the secondary spectrum $F(x,\lambda)$ the number and energy buildup factors are given by

$$B_N(x) = \int_{\lambda_o}^{\infty} e^{\mu_o x} F(x,\lambda)d\lambda$$

$$B_E(x) = \lambda_o \int_{\lambda_o}^{\infty} e^{\mu_o x} F(x,\lambda) \frac{d\lambda}{\lambda} . \qquad (5)$$

In Reference (2) it has been shown that solutions could be obtained to Eq. (3) if certain approximations were made for the dependence of μ on λ, and if the scattering kernel K were approximated by

$$K_1(\lambda',\lambda) = 2A\left(\frac{\lambda'}{\lambda}\right)^2 e^{\lambda'-\lambda} . \qquad (6)$$

The validity of Eq. (6) is discussed in Reference (2). With these assumptions, buildup factors were calculated for an initial energy of 20 mc^2 (10.2 Mev) for penetrations in lead out to 20 mean free paths. As shown in Reference (2) these results agreed much better with some exact calculations of Fano and Spencer than did the straight-ahead values. It was therefore felt worthwhile to extend the computations to cover a wider range of elements and initial energies. The values so obtained will be presented here, along with a brief mention of the significance of the phenomena exhibited by the results. A later report will treat in detail the explanation for buildup behavior.

Calculations

Buildup factors -- number and energy -- have been calculated for four substances: iron, tungsten, lead and uranium, at penetrations of 4, 7, 10, and 20 mean free paths (1 mean free path $\equiv 1/\mu_o$). For each substance source energies of 1 to 8 Mev have been considered. In addition buildup factors were calculated for a pure Compton scatterer at penetrations of 4, 8, 20, 30 and 40 mean free paths for 1 mc^2, 2.5 mc^2 and 10 mc^2 photons. A single geometry -- a plane monodirectional source -- has been used for all problems.

The cross section data for iron, tungsten, and lead were an adjusted version of data furnished by Mrs. Charlotte Davisson in a private communication [Reference (6)]. The data for tungsten were actually obtained by interpolating between tantalum and lead in Mrs. Davisson's data. For uranium the cross section data used were obtained from Reference (3), Supplement 1. The Compton scattering data were obtained from Reference (7).

For convenience representative data are assembled in Tables I and II. The cross sections are for elements of the following densities:

Element	Density (ρ = g/cm^3)
Iron	7.85
Tungsten	19.3
Lead	11.4
Uranium	18.7

TABLE I

Cross Section Data for Iron, Tungsten, Lead and Uranium

Energy (Mev)	Element*			
	Fe	W	Pb	U
0.25	0.945	9.25	6.675	14.549
0.50	0.652	2.540	1.750	3.815
1.00	0.468	1.255	0.792	1.537
2.00	0.336	0.834	0.511	0.879
3.00	0.281	0.760	0.467	0.808
4.00	0.258	0.760	0.471	0.827
6.00	0.237	0.819	0.516	0.879
8.00	0.234	0.900	0.560	0.935

* Cross sections are in cm^{-1} for densities listed in text.

TABLE II

Cross Section Data for a Pure Compton Scatterer

Energy (mc^2)	Total Microscopic Cross Section x 10^{24} in cm^2
0.5	0.3745
1.0	0.2866
2.0	0.2090
4.0	0.1446
6.0	0.1136
8.0	0.0947
10.0	0.0817

Analysis

The analytical work has been assembled in Appendix A. For convenience a glossary of the functions and parameters used in the R.M.S. procedure is presented below. A full discussion is contained in Reference (2).

$\phi(\lambda)$ is a logarithmic energy variable = $-\ell n(1+\lambda_o-\lambda)$

$\bar{\mu}(\lambda)$ is the effective R.M.S. cross section = $\frac{\mu(\lambda)}{1-(\lambda-\lambda_o)}$

$\bar{K}(\lambda',\lambda)$ is the effective R.M.S. scattering kernel = $\frac{K(\lambda',\lambda)}{1-(\lambda-\lambda_o)}$

g is the Greuling constant. If $\bar{K}(\lambda,\lambda) = g\frac{d\bar{\mu}}{d\lambda}$ in an energy interval then F can be expressed in terms of the confluent hypergeometric function. This equation is equivalent to requiring that $\bar{\mu}$ be a linear function of ϕ.

For a pure Compton scatterer Eq. (3), after an obvious change of variable, has been used in the form

$$\frac{\partial F}{\partial y} + \frac{m(\lambda)}{1-(\lambda-\lambda_o)} F(y,\lambda) = \int_{\lambda_o}^{\lambda} \frac{k(\lambda',\lambda)}{1-(\lambda'-\lambda_o)} F(y,\lambda')d\lambda' + k(\lambda_o,\lambda)e^{-y} \quad (7)$$

where

y is the number of mean free paths $\equiv \mu_o x$;

$m(\lambda) = \frac{\mu(\lambda)}{\mu_o} = \frac{\sigma(\lambda)}{\sigma_o}$. $\sigma(\lambda)$ is the total microscopic cross section, $\sigma_o = \sigma(\lambda_o)$;

$k(\lambda',\lambda) = 2\alpha\left(\frac{\lambda'}{\lambda}\right)^2 e^{\lambda'-\lambda}$, where $\alpha = \frac{A}{\mu_o} = \frac{\pi r_o^2}{\sigma_o}$; r_o is the classical electron radius = 2.80×10^{-13} cm.

In Appendix A are collected tables summarizing the analytic properties of the approximation for each problem, i.e. the appropriate g-value in each region, the subinterval in $\emptyset$, the piecewise linear approximation to the R.M.S. cross section, and finally the analytic solution. At the end of this Appendix are assembled several representative sketches of $\bar{\mu}$ versus $\emptyset$ and the piecewise approximations.

Effects of the Approximations to $\bar{\mu}$ and K

In order to test the effect of small variations in fitting $\bar{\mu}$ with linear functions of $\emptyset$, the case of 2 Mev γ-rays in tungsten was worked with three different such approximations. The crudest approximation has g = 1 and only one region. A better approximation has g = 0.735 and again only a single region. The third approximation, which was used to calculate the results reported in Appendix C, has two regions with respective g values of 1 and 1/2.

In the first approximation the analytic solution is

$$F = K(\lambda_o,\lambda)xe^{-\mu_o x}. \tag{8}$$

The second solution is

$$F = K(\lambda_o,\lambda)xe^{-\mu_o x}\,{}_1F_1\left[.265;2;(\mu_o-\bar{\mu})x\right]. \tag{9}$$

For the solution F in the third approximation see Appendix B, where the new Laplace inversion required for this situation has been worked out. Buildup factors in each of the three cases are recorded in Table III.

TABLE III

2 Mev Photons in Tungsten

	g=1		g=0.735		g=1, 1/2	
$\mu_o x$	B_N	B_E	B_N	B_E	B_N	B_E
4	1.77	1.12	1.41	1.00	1.48	1.03
7	3.10	1.95	2.29	1.64	2.55	1.79
10	4.43	2.79	3.10	2.24	3.61	2.54
20	8.86	5.58	5.53	4.09	7.14	5.05

The differences existing between the buildup factors obtained by the various approximations are probably representative of the deviations to be expected from the uncertainties in the piecewise approximation to the cross section. This type of calculation was not performed for each material or each energy. We are, however, confident that most of the stray points in Figures C6,...,C10 are attributable to fortuities in the fit. In this connection it should be pointed out that for most attenuation calculations an error of 25 percent in the buildup factor would be quite unimportant.

To determine the sensitivity of the buildup factors to changes in the kernel a different approximation than (6) was used in several cases. This alternative kernel is

$$K_2 = 2A\left(\frac{\lambda'}{\lambda}\right)^2 \qquad (10)$$

which differs from (6) in having no exponential dependence. This kernel has been used by Greuling and Welton [Reference (10)]. Here again the changes in the resulting buildup factors were relatively inconsequential ($\sim$ 20 percent in B_N; $\sim$ 15 percent in B_E). A representative comparison for both approximate kernels is exhibited in

Table IV for 5 Mev photons in uranium.

TABLE IV
5 Mev Photons in Uranium

	K_1		K_2	
$\mu_o x$	B_N	B_E	B_N	B_E
4	1.04	0.59	1.22	0.64
7	2.17	1.18	2.56	1.30
10	3.68	1.94	4.36	2.14
20	12.36	6.06	14.91	6.79

In estimating the relative merits of the two kernels, it should be noted that though K_2 approximates the exact kernel somewhat more closely than K_1 over a larger energy range, the latter is a better fit over the energy interval which is overwhelmingly more important in the R.M.S. theory, i.e. energies close to the initial energy. For this reason greater reliability is attributed to the results for $K \simeq K_1$.

Behavior of the Buildup Factors; Conclusions

Assembled in Appendix C are tables of the buildup factors for each of the elements, initial energies, and penetrations. The number buildups for the Compton scatterer are not included since this quantity, for a material in which no capture processes are taking place, is, of course,

$$B_N = e^{\mu_o x} - 1.$$

The R.M.S. calculation obviously cannot predict this quantity since it introduces, in effect, an artificial "capture" for all photons scattered 90° or more.

The behavior of the energy buildups with penetration in a heavy element (lead) is shown in Figures C1,...,C4. Figure C5 shows this behavior for a pure Compton scatterer.

In Figures C6,...,C10 are exhibited plots of buildup factors versus initial energies for the four substances and the pure Compton scatterer. The general trends are manifest. For substances of large atomic number ($Z \geq 74$) the buildups increase, achieve a broad maximum, and then decrease slowly for small and intermediate penetrations (< 10 mean free paths) but increase monotonically for large penetrations ($\sim$ 20 means free paths). For iron, on the other hand, the buildups decrease with energy, the rate of decrease falling off with diminishing penetration. This effect is accentuated in the pure Compton scatterer.

A detailed discussion of the physical reasons for these trends, and of the validity of the R.M.S. calculations will be presented in a subsequent report. It may be mentioned here, however, that it is felt that the decrease of the buildup with initial energy, for Compton scatterers, can be explained in terms of the nature of the energy degradation processes. At higher energies the scattered photons are very rapidly degraded to energies so low that they do not contribute appreciably to the buildup. This process is not nearly so marked at low initial energies, and the buildup is therefore relatively higher. With the heavier elements absorption

processes enter in addition to scattering. Thus at low initial energies absorption predominates and the buildup is correspondingly small. The photoelectric absorption decreases in proportion to scattering as E increases, and an increase in buildup for given penetration is therefore expected. It is believed that the variation for heavy elements can in large measure be explained by the varying proportion of absorption to scattering.

References

1. J. E. Wilkins, Jr., A. Oppenheim and L. Solon, The Transport Equation in the Straight-Ahead Case, NYO-633, September 1950
2. L. R. Solon and J. E. Wilkins, Jr., Straight-Ahead and Root-Mean-Square-Angle Calculations for 20 mc^2 γ-Rays in Lead, NYO-635, December 1950
3. W. S. Snyder and J. L. Powell, Absorption of γ-Rays, ORNL-421, March 1950
4. G. A. Campbell and R. M. Foster, Fourier Integrals for Practical Applications, D. van Nostrand Co., 1948
5. G. Young, Piece-Wise Greuling Solutions for Hydrogen, ORNL-415, September 1959
6. Charlotte Davisson, letter to H. Goldstein, December 1950
7. R. Latter and H. Kahn, Gamma-Ray Absorption Coefficients, RAND R-170, September 1949
8. S. O. Rice, Properties of a Sine Wave Plus Random Noise, Bell System Technical Journal, vol. 27, pp. 109-157, January 1948
9. J. E. Wilkins, Jr. and A. Oppenheim, Another Invertible Piece-wise Greuling Solution to the Straight-Ahead Transport Equation, NYO-638, April 1951
10. T. A. Welton, TID-256 (classified).
11. G. Placzek, The Functions $E_n(x) = \int_1^\infty e^{-xu} u^{-n} du$, MT-1, National Research Council of Canada, N.R.C. No. 1547, December 1946

Appendix A

TABLE A-I
R.M.S. Approximation for 1 Mev Photons in Uranium

Region	g	λ / ϕ-Interval	Cross Section Approximation	$F(x,\lambda)/K(\lambda_o,\lambda)$
I	.370	$.51 \leq \lambda \leq \infty$ $0 \leq \phi \leq \infty$	$\bar{\mu} = \frac{2A}{g}\phi + \mu_o$ $A = 1.072$ $\mu_o = 1.537$	$xe^{-\mu_o x}\,{}_1F_1\left[1-g;2;(\mu_o-\bar{\mu})x\right]$

TABLE A-II
R.M.S. Approximation for 2 Mev Photons in Uranium

Region	g	λ / ϕ-Interval	Cross Section Approximation	$F(x,\lambda)/K(\lambda_o,\lambda)$
I	.572	$.26 \leq \lambda \leq \infty$ $0 \leq \phi \leq \infty$	$\bar{\mu} = \frac{2A}{g}\phi + \mu_o$ $A = 1.072$ $\mu_o = .879$	$xe^{-\mu_o x}\,{}_1F_1\left[1-g;2;(\mu_o-\bar{\mu})x\right]$

TABLE A-III
R.M.S. Approximation for 3 Mev Photons in Uranium

Region	g	λ / ϕ-Interval	Cross Section Approximation	$F(x,\lambda)/K(\lambda_o,\lambda)$
I	+1	$.17 \leq \lambda \leq \infty$ $0 \leq \phi \leq \infty$	$A = 1.072$ $\mu_o = .808$	$xe^{-\mu_o x}$

TABLE A-IV
R.M.S. Approximation for 4 Mev Photons in Uranium

Region	g	λ / ϕ-Interval	Cross Section Approximation	$F(x,\lambda)/K(\lambda_o,\lambda)$
I	+2	$.13 \leq \lambda \leq .2142$ $0 \leq \phi \leq .088$	$\bar{\mu} = A\phi + \mu_o$ $A = 1.072$ $\mu_o = .827$	$xe^{-\mu_o x}\left[1+(\bar{\mu}-\mu_o)\frac{x}{2}\right]$
II	+1	$.2142 \leq \lambda \leq \infty$ $.088 \leq \phi \leq \infty$	$\bar{\mu}_1 = .921$	Replace $\bar{\mu}$ in Region I above by $\bar{\mu}_1$.

TABLE A-V

R.M.S. Approximation for 5 Mev Photons in Uranium

Region	g	$\frac{\lambda}{\emptyset}$-Interval	Cross Section Approximation	$F(x,\lambda)/K(\lambda_o,\lambda)$
I	+8	$.102 \leq \lambda \leq .186$ $0 \leq \emptyset \leq .088$	$\bar{\mu} = \frac{A}{4}\emptyset + \mu_o$ $A = 1.072$ $\mu_o = .847$	$\left\{ \frac{(\bar{\mu}-\mu_o)^7}{8!}x^8 + \frac{7(\bar{\mu}-\mu_o)^6}{7!}x^7 + \frac{21(\bar{\mu}-\mu_o)^5}{6!}x^6 + \frac{35(\bar{\mu}-\mu_o)^4}{5!}x^5 + \frac{35(\bar{\mu}-\mu_o)^3}{4!}x^4 + \frac{21(\bar{\mu}-\mu_o)^2}{3!}x^3 + \frac{7(\bar{\mu}-\mu_o)}{2!}x^2 + x\,e^{-\mu_o x} \right\}$
II	+1	$.186 \leq \lambda \leq \infty$ $.088 \leq \emptyset \leq \infty$	$\bar{\mu}_1 = .8706$	Replace $\bar{\mu}$ in Region I above by $\bar{\mu}_1$.

TABLE A-VI

R.M.S. Approximation for 6 Mev Photons in Uranium

Region	g	$\frac{\lambda}{\emptyset}$-Interval	Cross Section Approximation	$F(x,\lambda)/K(\lambda_o,\lambda)$
I	∞	$.085 \leq \lambda \leq .171$ $0 \leq \emptyset \leq .090$	$A = 1.072$ $\mu_o = .878$	$\sqrt{\frac{x}{\xi(\lambda)}}\, e^{-\mu_o x}\, I_1\left[2\sqrt{x\xi(\lambda)}\right]$ $\xi(\lambda) = 2A \ell n \frac{1}{1-(\lambda-\lambda_o)}$
II	+1	$.171 \leq \lambda \leq \infty$ $.090 \leq \emptyset \leq \infty$		Replace λ in Region I above by λ_1. $\lambda_1 = .171$.

TABLE A-VII

R.M.S. Approximation for 7 Mev Photons in Uranium

Region	g	$\frac{\lambda}{\emptyset}$-Interval	Cross Section Approximation	$F(x,\lambda)/K(\lambda_o,\lambda)$
I	-2	$.073 \leq \lambda \leq .098$ $0 \leq \emptyset \leq .025$	$\bar{\mu} = -A\emptyset + \mu_o$ $A = 1.072$ $\mu_o = .903$	$xe^{-\bar{\mu}x}\left[1+(\mu_o-\bar{\mu})\frac{x}{2}\right]$
II	∞	$.098 \leq \lambda \leq .159$ $.025 \leq \emptyset \leq .090$	$\bar{\mu}_1 = .876$	$(\mu_o-\bar{\mu}_1)\sqrt{\frac{x}{\xi(\lambda)}}\, e^{-\bar{\mu}_1 x} I_2(2\sqrt{x\xi(\lambda)})$ $+\sqrt{\frac{x}{\xi(\lambda)}}\, e^{-\bar{\mu}_1 x} I_1(2\sqrt{x\xi(\lambda)})$ $\xi(\lambda) = 2A\ell n \frac{1-(\lambda_1-\lambda_o)}{1-(\lambda-\lambda_o)}$ $\lambda_1 = .098$
III	+1	$.159 \leq \lambda \leq \infty$ $.090 \leq \emptyset \leq \infty$		Replace λ in Region II above by λ_2. $\lambda_2 = .159$.

TABLE A-VIII

R.M.S. Approximation for 8 Mev Photons in Uranium

Region	g	λ / $\emptyset$-Interval	Cross Section Approximation	$F(x,\lambda)/K(\lambda_o,\lambda)$
I	-2	$.064 \leq \lambda \leq .125$ $0 \leq \emptyset \leq .0625$	$\bar{\mu} = -A\emptyset + \mu_o$ $A = 1.072$ $\mu_o = .935$	$xe^{-\bar{\mu}x}\left[1+(\mu_o-\bar{\mu})\frac{x}{2}\right]$
II	+2	$.125 \leq \lambda \leq .201$ $.0625 \leq \emptyset \leq .1475$	$\bar{\mu} = A\emptyset + b$ $b = .801$ $\bar{\mu}_1 = .868$	$xe^{-\bar{\mu}_1 x}\left\{1+(\bar{\mu}+\mu_o+2\bar{\mu}_1)\frac{x}{2}\right.$ $\left.+(\bar{\mu}_1^2+\mu_o[\bar{\mu}-\bar{\mu}_1]-\bar{\mu}\bar{\mu}_1)\frac{x^2}{6}\right\}$
III	+1	$.201 \leq \lambda \leq \infty$ $.1475 \leq \emptyset \leq \infty$	$\bar{\mu}_2 = .959$	Replace $\bar{\mu}$ in Region II above by $\bar{\mu}_2$.

TABLE A-IX

R.M.S. Approximation for 1 Mev Photons in Lead

Region	g	$\frac{\lambda}{\emptyset}$-Interval	Cross Section Approximation	$F(x,\lambda)/K(\lambda_o,\lambda)$
I	$+\frac{1}{2}$	$.51 \leq \lambda \leq \infty$ $0 \leq \emptyset \leq \infty$	$\bar{\mu} = 4A\emptyset + \mu_o$ $A = .6692$ $\mu_o = .792$	$xe^{-\frac{1}{2}(\bar{\mu}+\mu_o)x}\left\{I_o\left[\frac{1}{2}(\bar{\mu}-\mu_o)x\right]\right.$ $\left. + I_1\left[\frac{1}{2}(\bar{\mu}-\mu_o)x\right]\right\}$

TABLE A-X

R.M.S. Approximation for 2 Mev Photons in Lead

Region	g	$\frac{\lambda}{\emptyset}$-Interval	Cross Section Approximation	$F(x,\lambda)/K(\lambda_o,\lambda)$
I	+.768	$.26 \leq \lambda \leq \infty$ $0 \leq \emptyset \leq \infty$	$\bar{\mu} = \frac{2A}{g}\emptyset + \mu_o$ $A = .6692$ $\mu_o = .511$	$xe^{-\mu_o x}\,{}_1F_1\left[1-g;2;(\mu_o-\bar{\mu})x\right]$

TABLE A-XI

R.M.S. Approximation for 3 Mev Photons in Lead

Region	g	$\frac{\lambda}{\emptyset}$-Interval	Cross Section Approximation	$F(x,\lambda)/K(\lambda_o,\lambda)$
I	+1	$.17 \leq \lambda \leq \infty$ $0 \leq \emptyset \leq \infty$	$A = .6692$ $\mu_o = .467$	$xe^{-\mu_o x}$

TABLE A-XII

R.M.S. Approximation for 4 Mev Photons in Lead

Region	g	λ / ϕ-Interval	Cross Section Approximation	$F(x,\lambda)/K(\lambda_o,\lambda)$
I	+2	$.13 \leq \lambda \leq .2115$ $0 \leq \phi \leq .085$	$\bar{\mu} = A\phi + \mu_o$ $A = .6692$ $\mu_o = .471$	$xe^{-\mu_o x}\left[1+(\bar{\mu}-\mu_o)\frac{x}{2}\right]$
II	+1	$.2115 \leq \lambda \leq \infty$ $.085 \leq \phi \leq \infty$	$\bar{\mu}_1 = .528$	Replace $\bar{\mu}$ in Region I above by $\bar{\mu}_1$.

TABLE A-XIII

R.M.S. Approximation for 5 Mev Photons in Lead

Region	g	λ / ϕ-Interval	Cross Section Approximation	$F(x,\lambda)/K(\lambda_o,\lambda)$
I	∞	$.102 \leq \lambda \leq .156$ $0 \leq \phi \leq .056$	$\mu_o = .492$	$\sqrt{\frac{x}{\xi(\lambda)}}\, e^{-\mu_o x} I_1\left[2\sqrt{x\xi(\lambda)}\right]$ $\xi(\lambda) = 2A \ell n \frac{1}{1-(\lambda-\lambda_o)}$
II	+2	$.156 \leq \lambda \leq .211$ $.056 \leq \phi \leq .115$	$\bar{\mu} = A\phi + b$ $A = .6692$ $b = .4545$	$e^{-\mu_o x}\left\{\frac{x}{\xi(\lambda_1)}(\bar{\mu}-\mu_o) I_2\left[2\sqrt{x\xi(\lambda_1)}\right] + \sqrt{\frac{x}{\xi(\lambda_1)}}\, I_1\left[2\sqrt{x\xi(\lambda_1)}\right]\right\}$
III	+1	$.211 \leq \lambda \leq \infty$ $.115 \leq \phi \leq \infty$	$\bar{\mu}_2 = .5315$	Replace $\bar{\mu}$ in Region II above by $\bar{\mu}_2$.

TABLE A-XIV

R.M.S. Approximation for 6 Mev Photons in Lead

Region	g	$\frac{\lambda}{\emptyset}$-Interval	Cross Section Approximation	$F(x,\lambda)/K(\lambda_o,\lambda)$
I	-2	$.085 \leq \lambda \leq .134$ $0 \leq \emptyset \leq .050$	$\bar{\mu} = -A\emptyset + \mu_o$ $A = .6692$ $\mu_o = .516$	$xe^{-\bar{\mu}x}\left[1+(\mu_o-\bar{\mu})\frac{x}{2}\right]$
II	+2	$.134 \leq \lambda \leq .198$ $.050 \leq \emptyset \leq .120$	$\bar{\mu} = A\emptyset + b$ $A = .6692$ $b = .449$ $\bar{\mu}_1 = .4825$	$xe^{-\bar{\mu}_1 x}\left\{1+(\bar{\mu}+\mu_o-2\bar{\mu}_1)\frac{x}{2}\right.$ $\left.+(\bar{\mu}_1^2+\mu_o[\bar{\mu}-\bar{\mu}_1]-\bar{\mu}\bar{\mu}_1)\frac{x^2}{6}\right\}$
III	+1	$.198 \leq \lambda \leq \infty$ $.120 \leq \emptyset \leq \infty$	$\bar{\mu}_2 = .529$	Replace $\bar{\mu}$ in Region II above by $\bar{\mu}_2$

TABLE A-XV

R.M.S. Approximation for 7 Mev Photons in Lead

Region	g	$\frac{\lambda}{\emptyset}$-Interval	Cross Section Approximation	$F(x,\lambda)/K(\lambda_o,\lambda)$
I	-2	$.073 \leq \lambda \leq .127$ $0 \leq \emptyset \leq .055$	$\bar{\mu} = -A\emptyset + \mu_o$ $A = .6692$ $\mu_o = .537$	$xe^{-\bar{\mu}x}\left[1+(\mu_o-\bar{\mu})\frac{x}{2}\right]$
II	+2	$.127 \leq \lambda \leq .206$ $.055 \leq \emptyset \leq .143$	$\bar{\mu}_1 = .500$	$xe^{-\bar{\mu}_1 x}\left\{1+(\bar{\mu}+\mu_o-2\bar{\mu}_1)\frac{x}{2}+(\bar{\mu}_1^2+\mu_o[\bar{\mu}-\bar{\mu}_1]-\bar{\mu}\bar{\mu}_1)\frac{x^2}{6}\right\}$
III	+1	$.206 \leq \lambda \leq \infty$ $.143 \leq \emptyset \leq \infty$	$\bar{\mu}_2 = .559$	Replace $\bar{\mu}$ in Region II above by $\bar{\mu}_2$

TABLE A-XVI

R.M.S. Approximation for 8 Mev Photons in Lead

Region	g	$\frac{\lambda}{\emptyset}$-Interval	Cross Section Approximation	$F(x,\lambda)/K(\lambda_o,\lambda)$
I	-1	$.064 \leq \lambda \leq .106$ $0 \leq \emptyset \leq .043$	$\bar{\mu} = -2A\emptyset + \mu_o$ $A = .6692$ $\mu_o = .560$	$xe^{-\bar{\mu}x}$
II	∞	$.106 \leq \lambda \leq .145$ $.043 \leq \emptyset \leq .084$	$\bar{\mu}_1 = .502$	$\sqrt{\frac{x}{\xi(\lambda)}}\, e^{-\bar{\mu}_1 x} I_1\left[2\sqrt{x\xi(\lambda)}\right]$ $\xi(\lambda) = 2A\ell n \frac{1-(\lambda_1-\lambda_o)}{1-(\lambda-\lambda_o)}$
III	+2	$.145 \leq \lambda \leq .205$ $.084 \leq \emptyset \leq .152$	$\bar{\mu} = A\emptyset + b$ $A = .6692$ $b = .446$	$e^{-\bar{\mu}_1 x}\left\{(\bar{\mu}-\bar{\mu}_1)\frac{x}{\xi(\lambda_2)} I_2\left[2\sqrt{x\xi(\lambda_2)}\right] + \sqrt{\frac{x}{\xi(\lambda_2)}} I_1\left[2\sqrt{x\xi(\lambda_2)}\right]\right\}$ $\lambda_2 = .145$
IV	+1	$.205 \leq \lambda \leq \infty$ $.152 \leq \emptyset \leq \infty$	$\bar{\mu}_3 = .548$	Replace $\bar{\mu}$ in Region III above by $\bar{\mu}_3$

TABLE A-XVII

R.M.S. Approximation for 1 Mev Photons in Tungsten

Region	g	$\frac{\lambda}{\emptyset}$-Interval	Cross Section Approximation	$F(x,\lambda)/K(\lambda_o,\lambda)$
I	+.591	$.51 \leq \lambda \leq \infty$ $0 \leq \emptyset \leq \infty$	$\bar{\mu} = \frac{2A}{g}\emptyset + \mu_o$ $A = 1.152$ $\mu_o = 1.255$	$xe^{-\mu_o x}\,{}_1F_1\left[1-g;2;(\mu_o-\bar{\mu})x\right]$

TABLE A-XVIII

R.M.S. Approximation for 2 Mev Photons in Tungsten

Region	g	$\frac{\lambda}{\emptyset}$-Interval	Cross Section Approximation	$F(x,\lambda)/K(\lambda_o,\lambda)$
I	+1	$.26 \leq \lambda \leq .48$ $0 \leq \emptyset \leq .247$	$A = 1.152$ $\mu_o = .890$	See Appendix B for analysis.
II	$+\frac{1}{2}$	$.48 \leq \lambda \leq \infty$ $.247 \leq \emptyset \leq \infty$	$\bar{\mu} = 4A\emptyset + b$ $b = .3209$	

TABLE A-XIX

R.M.S. Approximation for 3 Mev Photons in Tungsten

Region	g	$\frac{\lambda}{\emptyset}$-Interval	Cross Section Approximation	$F(x,\lambda)/K(\lambda_o,\lambda)$
I	+1	$.17 \leq \lambda \leq \infty$ $0 \leq \emptyset \leq \infty$	$A = 1.152$ $\mu_o = .760$	$xe^{-\mu_o x}$

TABLE A-XX

R.M.S. Approximation for 4 Mev Photons in Tungsten

Region	g	λ / ϕ-Interval	Cross Section Approximation	$F(x,\lambda)/K(\lambda_o,\lambda)$
I	+2	$.13 \leq \lambda \leq .1976$ $0 \leq \phi \leq .070$	$\bar{\mu} = A\phi + \mu_o$ $A = 1.152$ $\mu_o = .760$	$xe^{-\mu_o x}\left[1+(\bar{\mu}-\mu_o)\frac{x}{2}\right]$
II	+1	$.1976 \leq \lambda \leq \infty$ $.070 \leq \phi \leq \infty$	$\bar{\mu}_1 = .841$	Replace $\bar{\mu}$ in Region I above by $\bar{\mu}_1$.

TABLE A-XXI

R.M.S. Approximation for 5 Mev Photons in Tungsten

Region	g	λ / ϕ-Interval	Cross Section Approximation	$F(x,\lambda/K(\lambda_o,\lambda)$
I	∞	$.102 \leq \lambda \leq .138$ $0 \leq \phi \leq .037$	$\mu_o = .787$	$\sqrt{\frac{x}{\xi(\lambda)}}\, e^{-\mu_o x} I_1\left[2\sqrt{x\xi(\lambda)}\right]$ $\xi(\lambda) = 2A\ell n \frac{1}{1-(\lambda-\lambda_o)}$
II	+2	$.138 \leq \lambda \leq .203$ $.037 \leq \phi \leq .106$	$\bar{\mu} = A\phi + b$ $A = 1.152$ $b = .744$	$(\bar{\mu}-\mu_o)\frac{x}{\xi(\lambda_1)} e^{-\mu_o x} I_2\left[2\sqrt{x\xi(\lambda_1)}\right]$ $+\sqrt{\frac{x}{\xi(\lambda)}}\, e^{-\mu_o x} I_1\left[2\sqrt{x\xi(\lambda_1)}\right]$ $\lambda_1 = .138$
III	+1	$.203 \leq \lambda \leq \infty$ $.106 \leq \phi \leq \infty$	$\bar{\mu}_2 = .866$	Replace $\bar{\mu}$ in Region II above by $\bar{\mu}_2$.

TABLE A-XXII

R.M.S. Approximation for 6 Mev Photons in Tungsten

Region	g	λ ϕ-Interval	Cross Section Approximation	$F(x,\lambda)/K(\lambda_o,\lambda)$
I	∞	$.085 \leq \lambda \leq .18$ $0 \leq \phi \leq .100$	$A = 1.152$ $\mu_o = .819$	$\sqrt{\frac{x}{\xi(\lambda)}}\, e^{-\mu_o x}\, I_1\left[2\sqrt{x\xi(\lambda)}\right]$ $\xi(\lambda) = 2A \ln \frac{1}{1-(\lambda-\lambda_o)}$
II	+1	$.18 \leq \lambda \leq \infty$ $.100 \leq \phi \leq \infty$		Replace λ in Region I above by λ_1. $\lambda_1 = .18$.

TABLE A-XXIII

R.M.S. Approximation for 7 Mev Photons in Tungsten

Region	g	λ ϕ-Interval	Cross Section Approximation	$F(x,\lambda)/K(\lambda_o,\lambda)$
I	-1	$.073 \leq \lambda \leq .094$ $0 \leq \phi \leq .021$	$\bar{\mu} = -2A\phi + \mu_o$ $A = 1.152$ $\mu_o = .852$	$xe^{-\bar{\mu}x}$
II	∞	$.094 \leq \lambda \leq .134$ $.021 \leq \phi \leq .063$	$\bar{\mu}_1 = .804$	$\sqrt{\frac{x}{\xi(\lambda)}}\, e^{-\bar{\mu}_1 x}\, I_1\left[2\sqrt{x\xi(\lambda)}\right]$ $\xi(\lambda) = 2A \ln \frac{1-(\lambda_1-\lambda_o)}{1-(\lambda-\lambda_o)}$
III	+2	$.134 \leq \lambda \leq .195$ $.063 \leq \phi \leq .130$	$\bar{\mu} = A\phi + b$ $A = 1.152$ $b = .731$	$e^{-\mu_o x}\left\{\frac{(\bar{\mu}-\bar{\mu}_1)x I_2\left[2\sqrt{x\xi(\lambda_2)}\right]}{\xi(\lambda_2)}\right.$ $\left. + \sqrt{\frac{x}{\xi(\lambda_2)}}\, I_1\left[2\sqrt{x\xi(\lambda_2)}\right]\right\}$ $\lambda_2 = .134$
IV	+1	$.195 \leq \lambda \leq \infty$ $.130 \leq \phi \leq \infty$	$\bar{\mu}_3 = .881$	Replace $\bar{\mu}$ in Region III above by $\bar{\mu}_3$.

TABLE A-XXIV

R.M.S. Approximation for 8 Mev Photons in Tungsten

Region	g	λ / $\emptyset$-Interval	Cross Section Approximation	$F(x,\lambda)/K(\lambda_o,\lambda)$
I	-1	$.064 \leq \lambda \leq .111$ $0 \leq \emptyset \leq .048$	$\bar{\mu} = A\emptyset + \mu_o$ $A = 1.152$ $\mu_o = .900$	$xe^{-\bar{\mu}x}$
II	+2	$.111 \leq \lambda \leq .203$ $.048 \leq \emptyset \leq .15$	$\bar{\mu} = A\emptyset + b$ $A = 1.152$ $b = .734$ $\bar{\mu}_1 = .789$	$xe^{-\bar{\mu}_1 x}\left[1 + \frac{x}{2}(\bar{\mu}-\bar{\mu}_1)\right]$
III	+1	$.203 \leq \lambda \leq \infty$ $.15 \leq \emptyset \leq \infty$	$\bar{\mu}_2 = .907$	Replace $\bar{\mu}$ in Region II above by $\bar{\mu}_2$.

TABLE A-XXV

R.M.S. Approximation for 1 Mev Photons in Iron

Region	g	λ / ϕ-Interval	Cross Section Approximation	$F(x,\lambda)/K(\lambda_o,\lambda)$
I	+1	$.51 \leq \lambda \leq \infty$ $0 \leq \phi \leq \infty$	$A = .5421$ $\mu_o = .468$	$xe^{-\mu_o x}$

TABLE A-XXVI

R.M.S. Approximation for 2 Mev Photons in Iron

Region	g	λ / ϕ-Interval	Cross Section Approximation	$F(x,\lambda)/K(\lambda_o,\lambda)$
I	+1	$.26 \leq \lambda \leq \infty$ $0 \leq \phi \leq \infty$	$A = .5421$ $\mu_o = .336$	$xe^{-\mu_o x}$

TABLE A-XXVII

R.M.S. Approximation for 3 Mev Photons in Iron

Region	g	λ / ϕ-Interval	Cross Section Approximation	$F(x,\lambda)/K(\lambda_o,\lambda)$
I	+1	$.17 \leq \lambda \leq \infty$ $0 \leq \phi \leq \infty$	$A = .5421$ $\mu_o = .281$	$xe^{-\mu_o x}$

TABLE A-XXVIII

R.M.S. Approximation for 4 Mev Photons in Iron

Region	g	λ / ϕ-Interval	Cross Section Approximation	$F(x,\lambda)/K(\lambda_o,\lambda)$
I	$+\frac{3}{2}$	$.13 \leq \lambda \leq .17$ $0 \leq \phi \leq .043$	$\bar{\mu} = \frac{4}{3} A\phi + \mu_o$ $A = .5421$ $\mu_o = .258$	$\frac{x}{3} e^{-(\bar{\mu}+\mu_o)\frac{x}{2}} \left\{ \left[3+2(\bar{\mu}-\mu_o)x \right] I_o \left[(\bar{\mu}-\mu_o)\frac{x}{2} \right] + \left[1+2(\bar{\mu}-\mu_o)x \right] I_1 \left[(\bar{\mu}-\mu_o)\frac{x}{2} \right] \right\}$
II	+1	$.17 \leq \lambda \leq \infty$ $.043 \leq \phi \leq \infty$	$\bar{\mu}_1 = .289$	Replace $\bar{\mu}$ in Region I above by $\bar{\mu}_1$.

TABLE A-XXIX

R.M.S. Approximation for 5 Mev Photons in Iron

Region	g	$\frac{\lambda}{\emptyset}$-Interval	Cross Section Approximation	$F(x,\lambda)/K(\lambda_o,\lambda)$
I	+2	$.102 \leq \lambda \leq .1412$ $0 \leq \emptyset \leq .040$	$\bar{\mu} = A\emptyset + \mu_o$ $A = .5421$ $\mu_o = .246$	$xe^{-\mu_o x}\left[1+(\bar{\mu}-\mu_o)\frac{x}{2}\right]$
II	+1	$.1412 \leq \lambda \leq \infty$ $.040 \leq \emptyset \leq \infty$	$\bar{\mu}_1 = .268$	Replace $\bar{\mu}$ in Region I above by $\bar{\mu}_1$.

TABLE A-XXX

R.M.S. Approximation for 6 Mev Photons in Iron

Region	g	$\frac{\lambda}{\emptyset}$-Interval	Cross Section Approximation	$F(x,\lambda)/K(\lambda_o,\lambda)$
I	+2	$.085 \leq \lambda \leq .1242$ $0 \leq \emptyset \leq .040$	$\bar{\mu} = A\emptyset + \mu_o$ $A = .5421$ $\mu_o = .237$	$xe^{-\mu_o x}\left[1+(\bar{\mu}-\mu_o)\frac{x}{2}\right]$
II	+1	$.1242 \leq \lambda \leq \infty$ $.040 \leq \emptyset \leq \infty$	$\bar{\mu}_1 = .259$	Replace $\bar{\mu}$ in Region I above by $\bar{\mu}_1$.

TABLE A-XXXI

R.M.S. Approximation for 7 Mev Photons in Iron

Region	g	λ / ϕ-Interval	Cross Section Approximation	$F(x,\lambda)/K(\lambda_o,\lambda)$
I	+2	$.073 \leq \lambda \leq .1284$ $0 \leq \phi \leq .057$	$\bar{\mu} = A\phi + \mu_o$ $A = .5421$ $\mu_o = .2345$	$xe^{-\mu_o x}\left[1+(\bar{\mu}-\mu_o)\frac{x}{2}\right]$
II	+1	$.1284 \leq \lambda \leq \infty$ $.057 \leq \phi \leq \infty$	$\bar{\mu}_1 = .265$	Replace $\bar{\mu}$ in Region I above by $\bar{\mu}_1$.

TABLE A-XXXII

R.M.S. Approximation for 8 Mev Photons in Iron

Region	g	λ / ϕ-Interval	Cross Section Approximation	$F(x,\lambda)/K(\lambda_o,\lambda)$
I	+2	$.064 \leq \lambda \leq .158$ $0 \leq \phi \leq .099$	$\bar{\mu} = A\phi + \mu_o$ $A = .5421$ $\mu_o = .234$	$xe^{-\mu_o x}\left[1+(\bar{\mu}-\mu_o)\frac{x}{2}\right]$
II	+1	$.158 \leq \lambda \leq \infty$ $.099 \leq \phi \leq \infty$	$\bar{\mu}_1 = .288$	Replace $\bar{\mu}$ in Region I above by $\bar{\mu}_1$.

TABLE A-XXXIII
R.M.S. Approximation for 1 mc^2 Photons
in a Pure Compton Scatterer

Region	g	λ / ϕ-Interval	Cross Section Approximation	$F(y,\lambda)/k(\lambda_o,\lambda)$
I	+1	$1.0 \leq \lambda \leq \infty$ $0 \leq \phi \leq \infty$	$\bar{m} = 2a\phi + 1$ $a = .8594$ $\sigma_o = .2866 \times 10^{-24} cm^2$	ye^{-y}

TABLE A-XXXIV
R.M.S. Approximation for 2.5 mc^2 Photons
in a Pure Compton Scatterer

Region	g	λ / ϕ-Interval	Cross Section Approximation	$F(y,\lambda)/k(\lambda_o,\lambda)$
I	+1	$0.4 \leq \lambda \leq \infty$ $0 \leq \phi \leq \infty$	$\bar{m} = 2a\phi + 1$ $a = 1.3185$ $\sigma_o = .1868 \times 10^{-24} cm^2$	ye^{-y}

TABLE A-XXXV
R.M.S. Approximation for 10 mc^2 Photons
in a Pure Compton Scatterer

Region	g	λ / ϕ-Interval	Cross Section Approximation	$F(y,\lambda)/k(\lambda_o,\lambda)$
I	+.928	$0.1 \leq \lambda \leq \infty$ $0 \leq \phi \leq \infty$	$\bar{m} = \frac{2a\phi}{g} + 1$ $a = 3.0147$ $\sigma_o = .0817 \times 10^{-24} cm^2$	$ye^{-y}\,{}_1F_1\left[1-g;2;(1-\bar{m})y\right]$

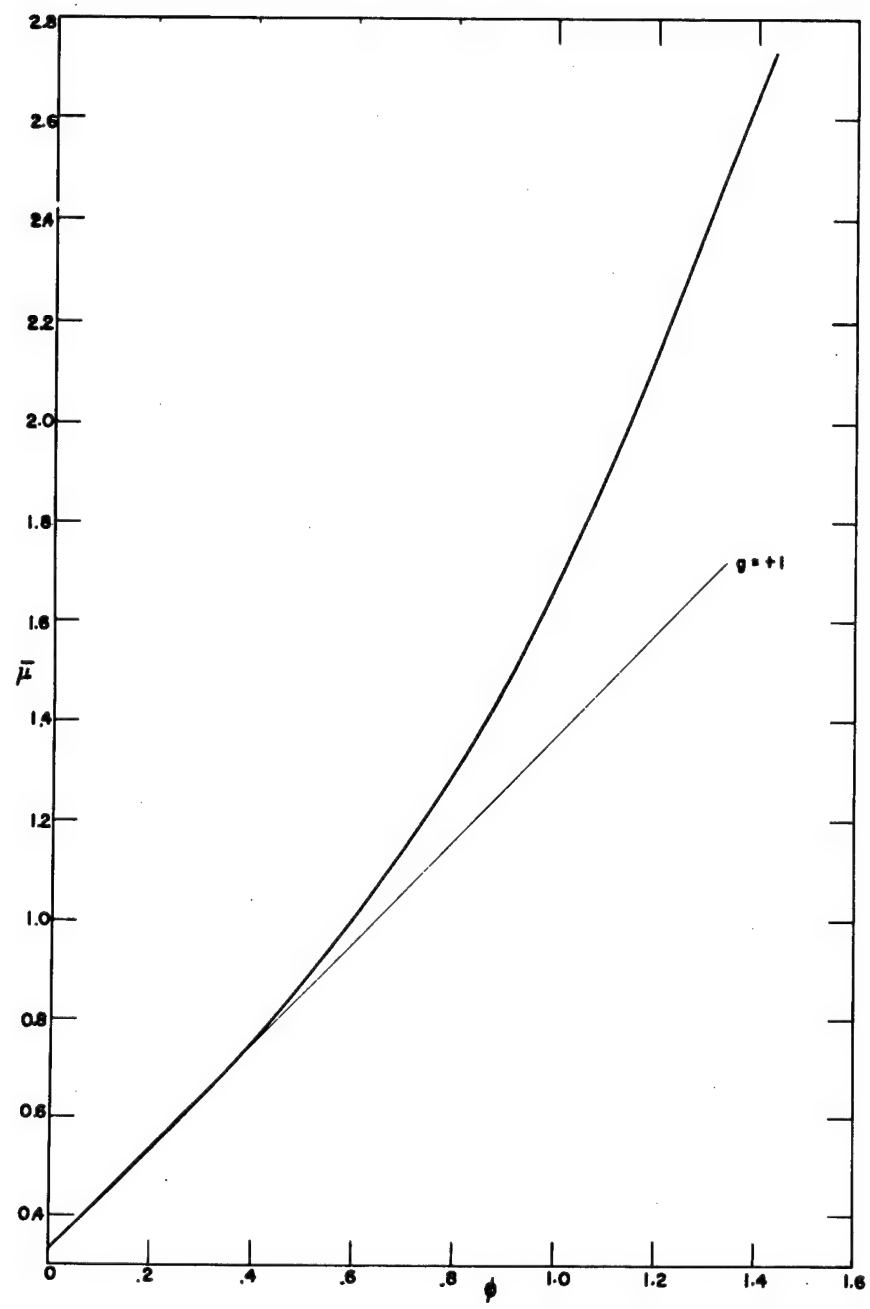

Figure A1 — Piecewise approximation to the R.M.S. cross section for 2 Mev photons in iron.

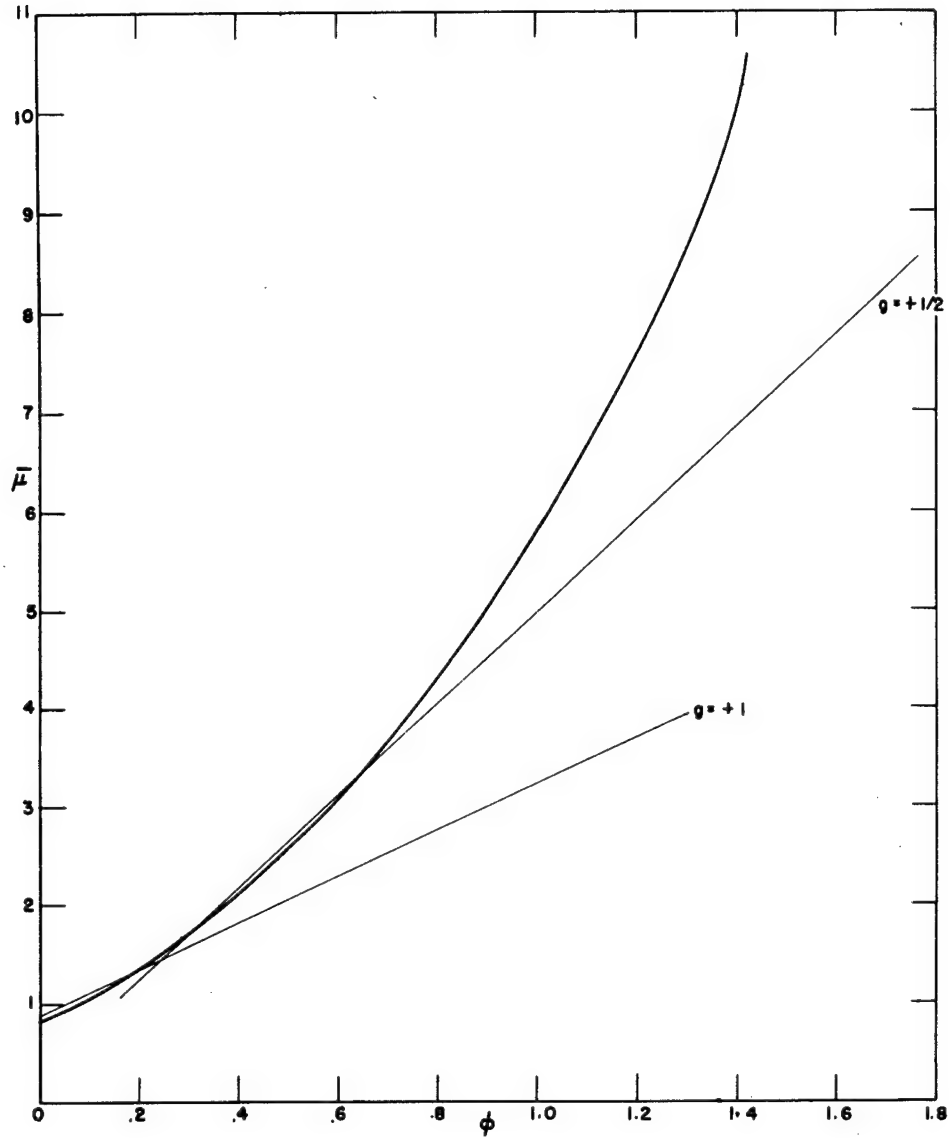

Figure A2 — Piecewise approximation to the R.M.S. cross section for 2 Mev photons in tungsten.

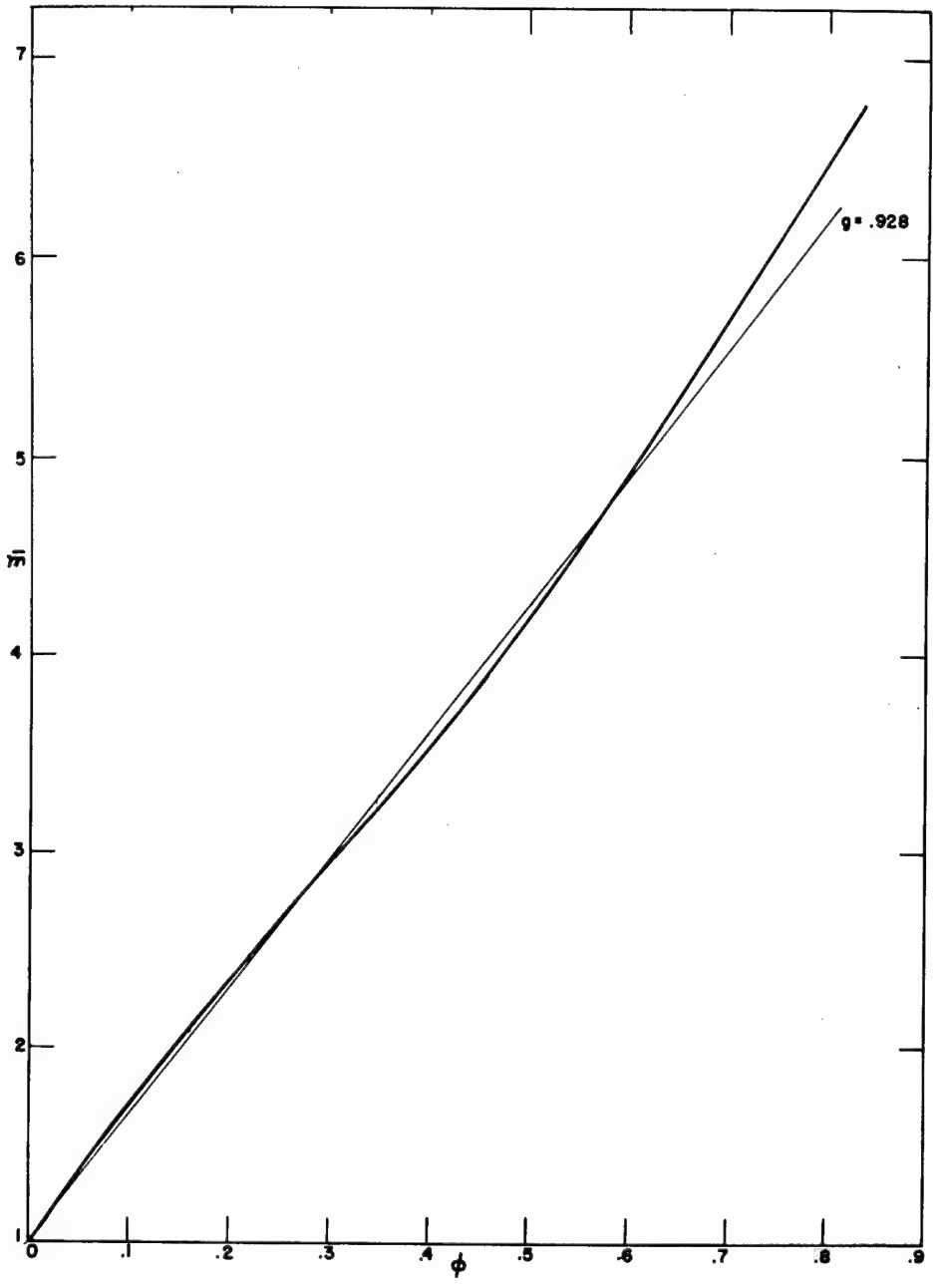

Figure A3 — Piecewise approximation to the R.M.S. cross section for 10 mc^2 photons in a pure Compton scatterer.

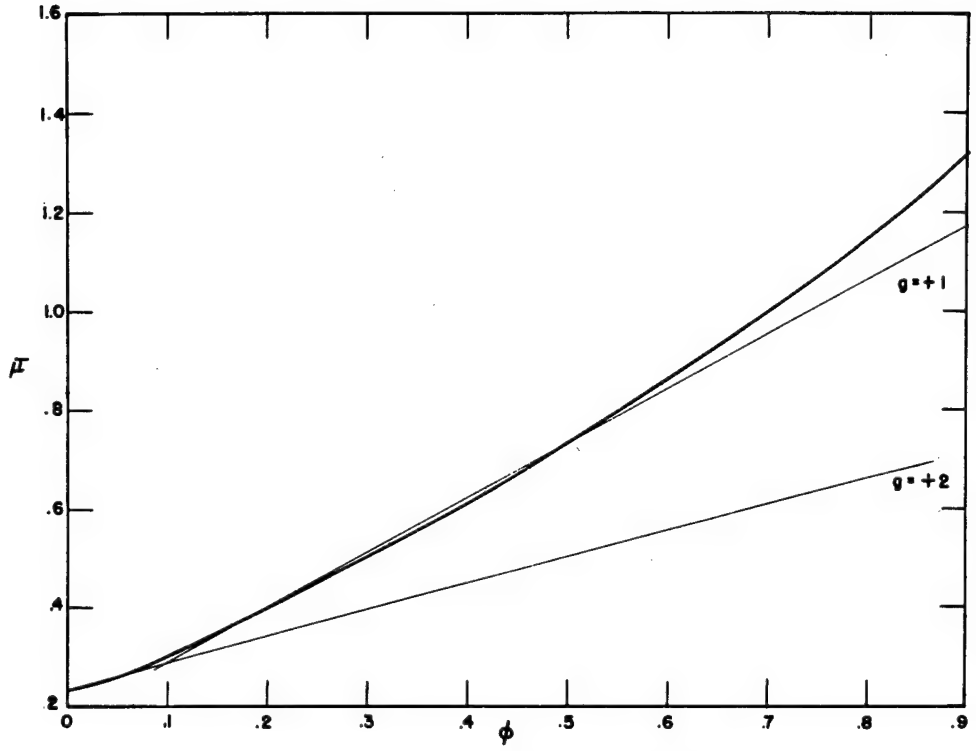

Figure A4 — Piecewise approximation to the R.M.S. cross section for 5 Mev photons in iron.

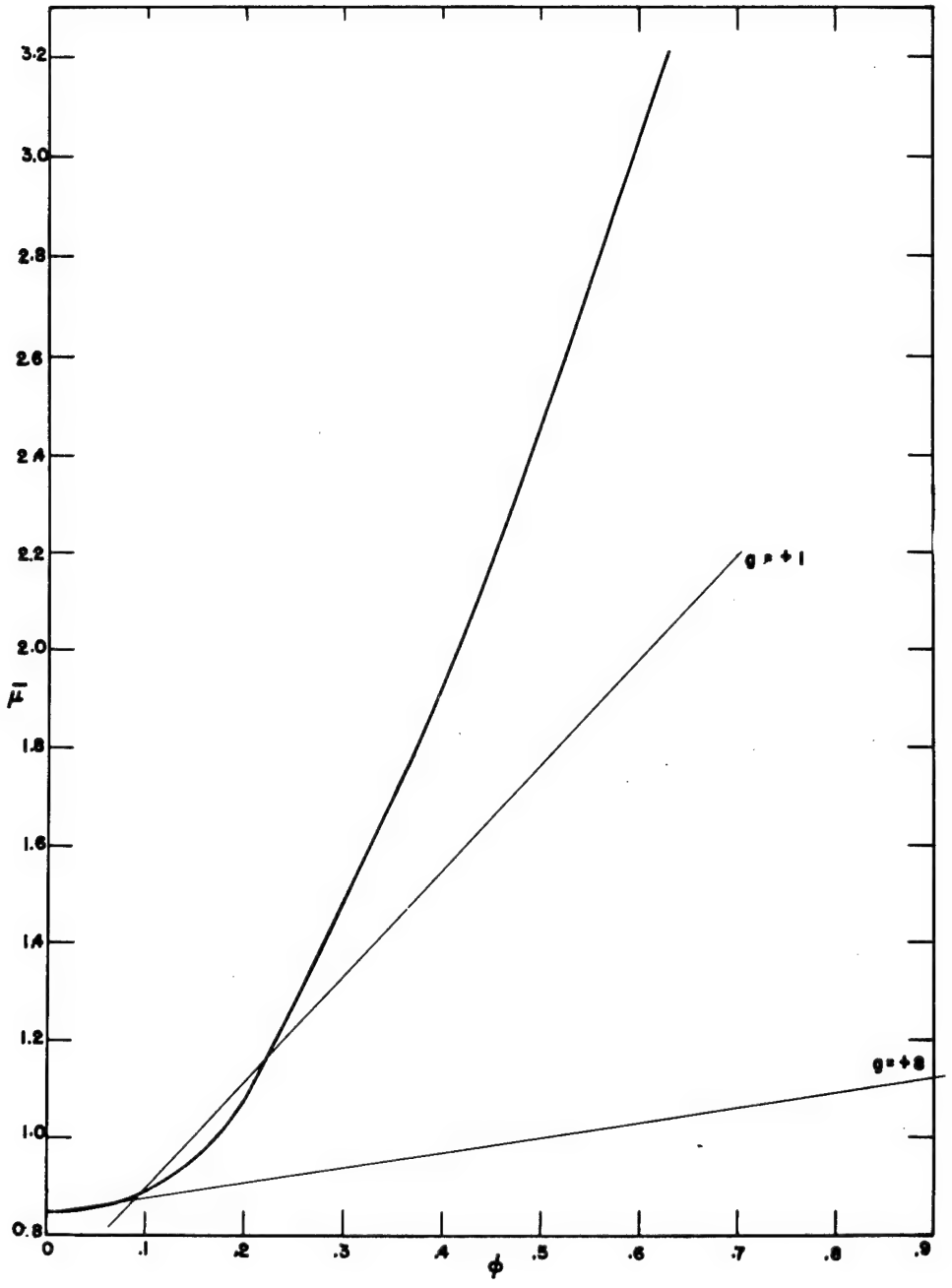

Figure A5 — Piecewise approximation to the R.M.S. cross section for 5 Mev photons in uranium.

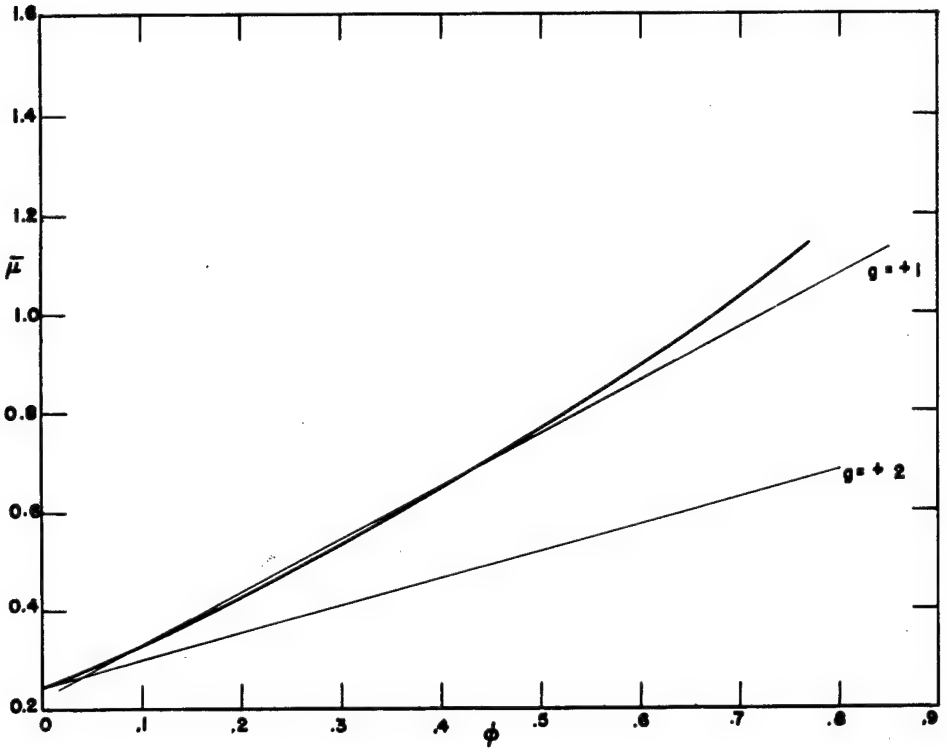

Figure A6 — Piecewise approximation to the R.M.S. cross section for 8 Mev photons in iron.

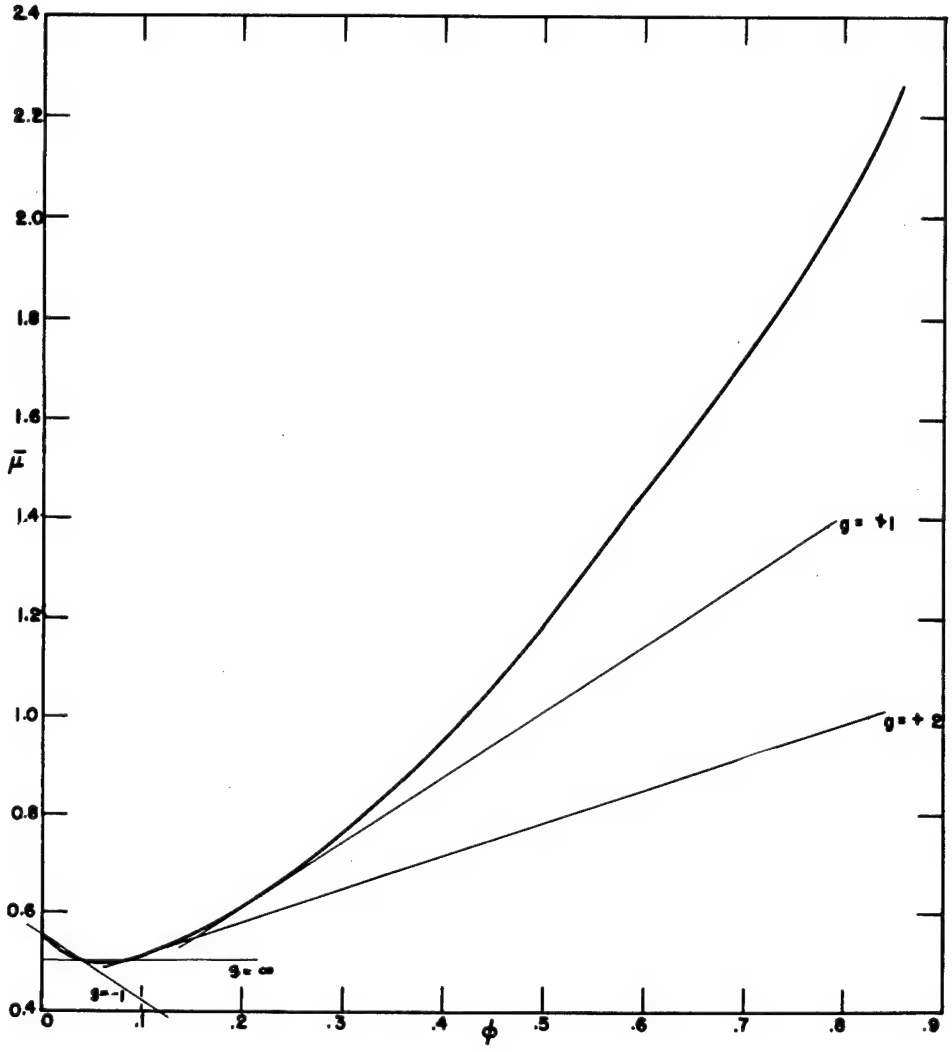

Figure A7 — Piecewise approximation to the R.M.S. cross section for 8 Mev photons in lead.

Appendix B

It is known that if $\bar{K}(\lambda',\lambda)$ is separable, i.e. factorable as a product $L(\lambda')M(\lambda)$, the result of applying a Laplace transform to a function $F(x,\lambda)$ which satisfies Eq. (3) is [Reference (1)]

$$f(s,\lambda) = \frac{K(\lambda_o,\lambda)}{(\mu_o+s)(\bar{\mu}+s)} \exp \int_{\lambda_o}^{\lambda} \frac{\bar{K}(\lambda',\lambda')d\lambda'}{\bar{\mu}(\lambda')+s} . \tag{B1}$$

Suppose it is true that there is a number λ_1 such that

$$\begin{aligned} \bar{K}(\lambda,\lambda) &= \frac{d\bar{\mu}}{d\lambda} && (\lambda_o \leqq \lambda < \lambda_1), \\ \bar{K}(\lambda,\lambda) &= \frac{1}{2}\frac{d\bar{\mu}}{d\lambda} && (\lambda_1 < \lambda). \end{aligned} \tag{B2}$$

By virtue of the definitions of $\bar{K}$ and ϕ, these equations can also be written as follows:

$$\begin{aligned} K(\lambda,\lambda) &= \frac{d\bar{\mu}}{d\phi} && (0 \leqq \phi < \phi_1), \\ K(\lambda,\lambda) &= \frac{1}{2}\frac{d\bar{\mu}}{d\phi} && (\phi_1 < \phi), \end{aligned} \tag{B3}$$

in which $\phi_1 = -\ell n(1+\lambda_o-\lambda_1)$. Then it is clear that

$$f(s,\lambda) = \frac{K(\lambda_o,\lambda)}{(\mu_o+s)^2} \qquad (\lambda_o \leqq \lambda \leqq \lambda_1), \tag{B4}$$

$$f(s,\lambda) = \frac{K(\lambda_o,\lambda)(\bar{\mu}_1+s)^{1/2}}{(\mu_o+s)^2(\bar{\mu}+s)^{1/2}} \qquad (\lambda_1 \leqq \lambda),$$

in which $\bar{\mu}_1 = \bar{\mu}(\lambda_1)$, and so [Reference (4), No. 442]

$$F(x,\lambda) = K(\lambda_o,\lambda)xe^{-\mu_o x} \qquad (\lambda_o \leqq \lambda \leqq \lambda_1). \tag{B5}$$

To determine $F(x,\lambda)$ when $\lambda \geq \lambda_1$, we observe that

$$\frac{f(s,\lambda)}{K(\lambda_o,\lambda)} = -\frac{\partial}{\partial\mu_o}\left\{\frac{\bar{\mu}_1-\mu_o}{(\mu_o+s)(\bar{\mu}_1+s)^{1/2}(\bar{\mu}+s)^{1/2}}\right\}, \tag{B6}$$

and hence [Reference (4), No. 219, No. 555]

$$\frac{F(x,\lambda)}{K(\lambda_o,\lambda)} = -\frac{\partial}{\partial\mu_o}\left\{(\bar{\mu}_1-\mu_o)e^{-\mu_o x}\int_0^x e^{\mu_o y}e^{-\frac{1}{2}(\bar{\mu}_1+\bar{\mu})y}I_o\left[\tfrac{1}{2}(\bar{\mu}_1-\bar{\mu})y\right]dy\right\}. \tag{B7}$$

After a little manipulation, this reduces to

$$\frac{e^{\mu_o x}F(x,\lambda)}{K(\lambda_o,\lambda)} = \int_0^x e^{-y(\bar{\mu}_1+\bar{\mu}-2\mu_o)/2}I_o\left[\tfrac{1}{2}(\bar{\mu}_1-\bar{\mu})y\right]\left[1+(\bar{\mu}_1-\mu_o)x\right]dy$$
$$- (\bar{\mu}_1-\mu_o)\int_0^x ye^{-y(\bar{\mu}_1+\bar{\mu}-2\mu_o)/2}I_o\left[\tfrac{1}{2}(\bar{\mu}_1-\bar{\mu})y\right]dy. \tag{B8}$$

Let us now define a function $G(k,v)$ by the integral

$$G(k,v) = \int_0^v e^{-u}I_o(ku)du. \tag{B9}$$

This function has been found useful in other applications [Reference (8)]. It has been studied and tabulated elsewhere [References (8) and (9)]. The only property of this function which we need here is the following [Reference (9)]:

$$(1-k^2)\int_0^v ue^{-u}I_o(ku)du = G(k,v) - ve^{-v}\left[I_o(kv) + kI_1(kv)\right]. \tag{B10}$$

In terms of this function G, it is now clear that

$$\frac{e^{\mu_o x} F(x,\lambda)}{K(\lambda_o,\lambda)} = \frac{2}{\bar{\mu}+\bar{\mu}_1-2\mu_o}\left\{(1 - \frac{2h}{1-k^2} + 2hv)G(k,v) + \frac{2hve^{-v}\left[I_o(kv) + kI_1(kv)\right]}{1-k^2}\right\}, \tag{B11}$$

in which

$$h = \frac{\bar{\mu}_1-\mu_o}{\bar{\mu}+\bar{\mu}_1-2\mu_o}\ ,\quad k = \frac{\bar{\mu}-\bar{\mu}_1}{\bar{\mu}+\bar{\mu}_1-2\mu_o}\ ,\quad v = \frac{1}{2}\ (\bar{\mu}+\bar{\mu}_1-2\mu_o)x\ . \tag{B12}$$

The tables of Reference (8) are inadequate for the computations reported in Appendix C of this report and so it is necessary to make use of the approximation [Reference (9)]

$$G(k,v) = (1-k^2)^{-1/2} - \frac{1}{4k}\left\{\frac{e^{-(1-k)v}}{(2\pi kv)^{1/2}} + \frac{(5k-1)\left[1-H(\sqrt{(1-k)v})\right]}{\left[2k(1-k)\right]^{1/2}}\right\}, \tag{B13}$$

valid for k near one and v large, in which H(t) is the error function

$$H(t) = \frac{2}{\sqrt{\pi}}\int_0^t e^{-u^2}du.$$

Appendix C

TABLE C-I
Buildup Factors for Uranium (ρ = 18.7 g/cm^3)

Initial Energy (Mev)	Penetration ($\mu_o x$) 4		7		10		20	
	B_N	B_E	B_N	B_E	B_N	B_E	B_N	B_E
1	0.74	0.60	1.06	0.87	1.32	1.11	2.06	1.78
2	1.07	0.79	1.66	1.25	2.18	1.67	3.71	2.93
3	1.31	0.79	2.29	1.38	3.27	1.97	6.54	3.95
4	1.17	0.69	2.25	1.31	3.51	2.05	9.02	5.01
5	1.04	0.59	2.17	1.18	3.68	1.94	12.36	6.06
6	0.89	0.48	1.88	0.98	3.26	1.64	12.03	5.45
7	1.04	0.50	2.18	1.02	3.71	1.70	12.85	5.46
8	0.71	0.36	1.63	0.78	3.08	1.38	15.94	6.02

TABLE C-II
Buildup Factors for Lead (ρ = 11.4 g/cm^3)

Initial Energy (Mev)	Penetration ($\mu_o x$) 4		7		10		20	
	B_N	B_E	B_N	B_E	B_N	B_E	B_N	B_E
1	1.03	0.81	1.54	1.23	1.98	1.60	3.19	2.64
2	1.39	0.97	2.28	1.62	3.11	2.22	5.62	4.10
3	1.41	0.85	2.47	1.49	3.53	2.13	7.06	4.26
4	1.29	0.76	2.50	1.45	3.93	2.25	10.33	5.71
5	1.16	0.80	2.51	1.34	4.37	2.26	16.16	7.73
6	1.04	0.55	2.40	1.21	4.54	2.19	23.16	9.95
7	0.88	0.46	2.06	1.00	3.93	1.81	20.74	8.28
8	0.81	0.41	1.84	0.88	4.38	1.85	34.63	12.06

TABLE C-III
Buildup Factors for Tungsten (ρ = 19.3 g/cm^3)

Initial Energy (Mev)	Penetration ($\mu_o x$) 4		7		10		20	
	B_N	B_E	B_N	B_E	B_N	B_E	B_N	B_E
1	1.10	0.86	1.65	1.32	2.11	1.71	3.41	2.82
2	1.48	1.03	2.55	1.79	3.61	2.54	7.14	5.05
3	1.50	0.90	2.62	1.58	3.74	2.26	7.49	4.52
4	1.35	0.80	2.80	1.61	4.10	2.37	11.08	5.92
5	1.22	0.68	2.58	1.40	4.40	2.33	15.11	7.49
6	1.09	0.58	2.42	1.23	4.38	2.11	18.45	7.89
7	0.97	0.51	2.32	1.14	4.46	2.08	31.58	10.21
8	0.87	0.44	2.19	1.02	4.58	1.98	37.74	12.61

TABLE C-IV
Buildup Factors for Iron (ρ = 7.85 g/cm^3)

Initial Energy (Mev)	Penetration ($\mu_o x$) 4		7		10		20	
	B_N	B_E	B_N	B_E	B_N	B_E	B_N	B_E
1	2.53	1.72	4.42	3.01	6.32	4.30	12.64	8.59
2	2.21	1.39	3.86	2.43	5.52	3.48	11.04	6.95
3	1.91	1.15	3.34	2.01	4.76	2.87	9.53	5.75
4	1.81	1.08	3.36	2.00	5.07	3.00	11.77	6.88
5	1.63	0.95	3.12	1.80	4.83	2.77	12.20	6.86
6	1.46	1.00	2.79	1.59	4.33	2.44	10.95	6.03
7	1.34	0.75	2.61	1.43	4.12	2.22	10.83	5.62
8	1.27	0.69	2.55	1.34	4.10	2.09	11.31	5.30

TABLE C-V
Energy Buildup Factors for a Pure Compton Scatterer

Initial Energy (mc^2)	B_E Penetration ($\mu_o x$) 4	8	20	30	40
1.0	2.05	4.10	10.25	15.38	20.50
2.5	1.62	3.24	8.10	12.15	16.19
10.0	1.24	2.45	6.00	8.92	11.81

* * * *

The buildup factors exhibited here have been obtained by numerical integration of the function $F(x,\lambda)$ except for those single region cases in which g = +1. Here the integrations were performed analytically with the help of the incomplete gamma functions tabulated in Reference (11).

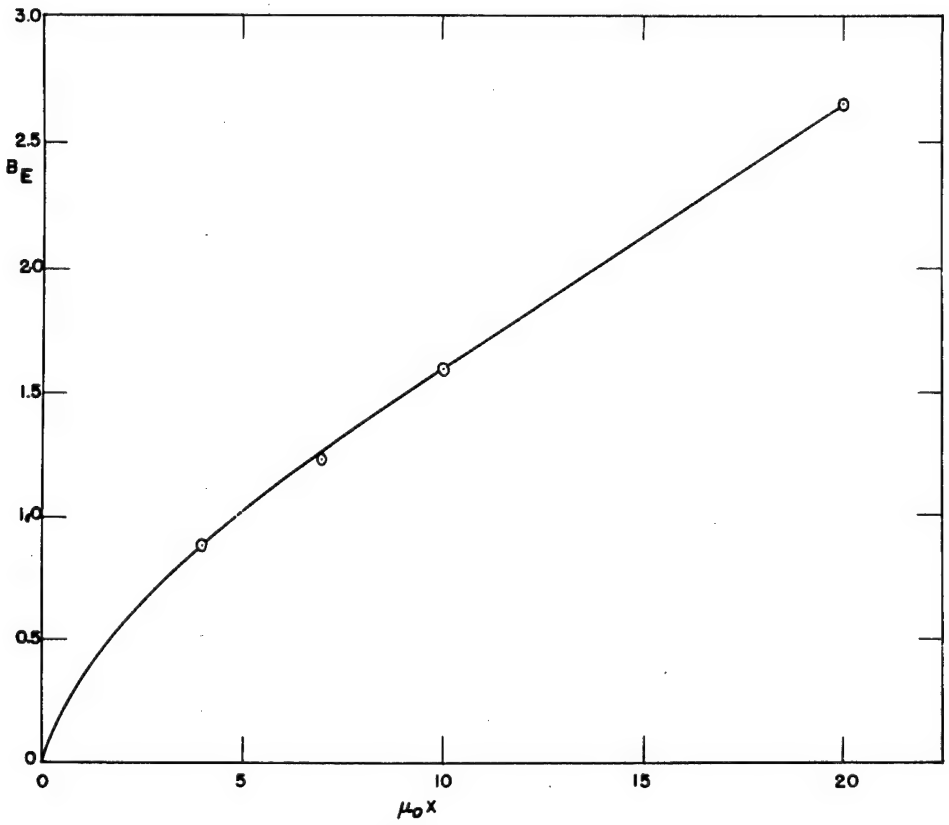

Figure C1 — Energy buildups vs. penetration; 1 Mev photons in lead.

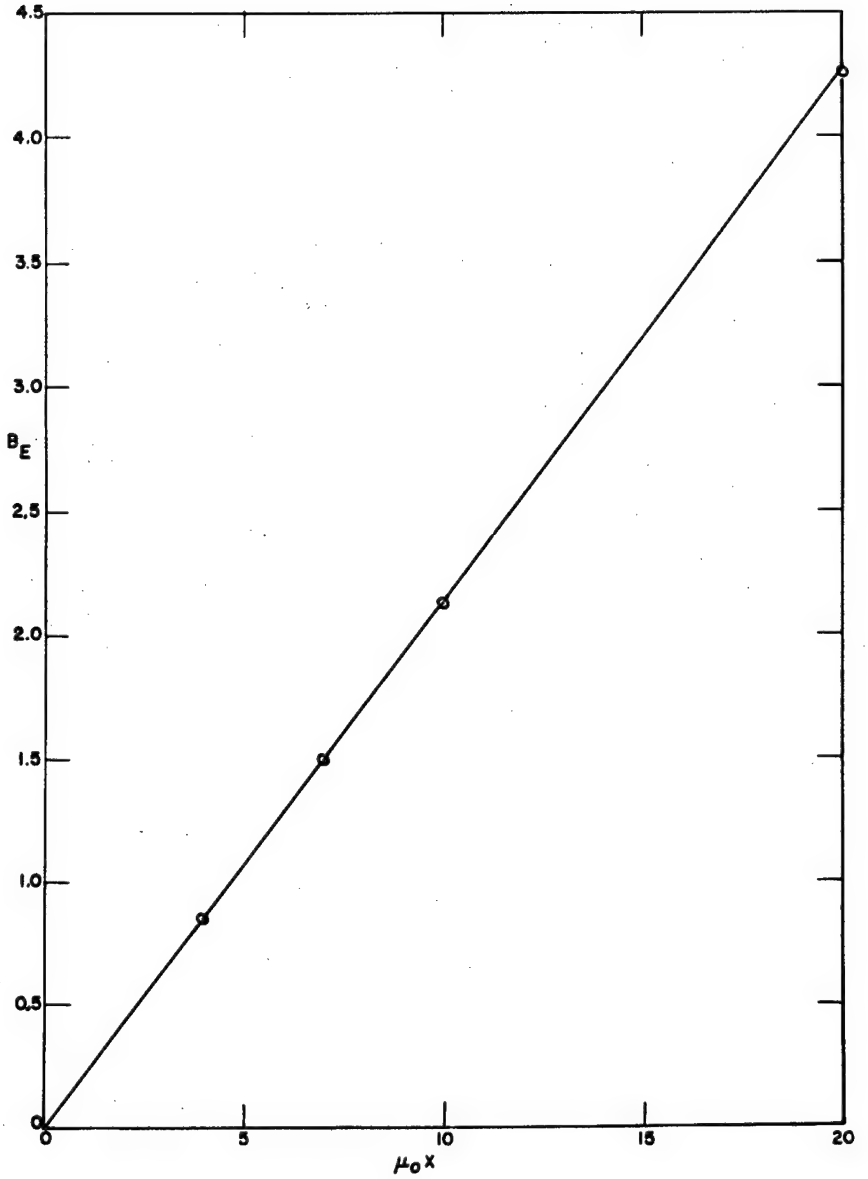

Figure C2 — Energy buildups vs. penetration; 3 Mev photons in lead.

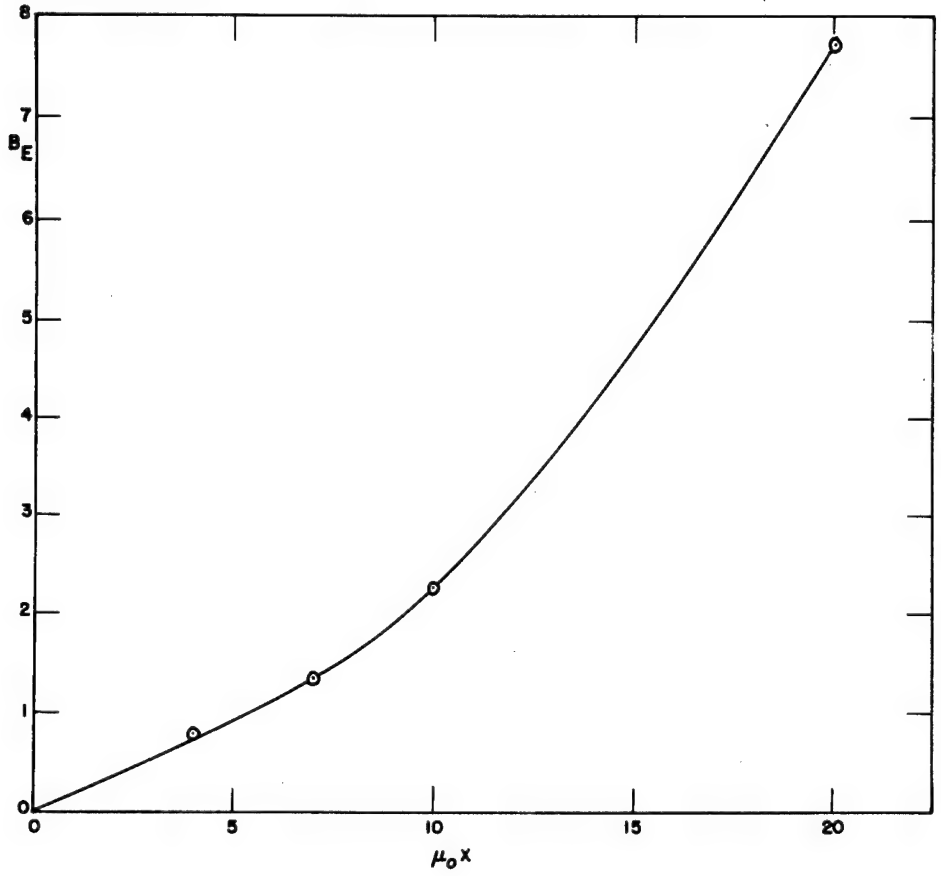

Figure C3 — Energy buildups vs. penetration; 5 Mev photons in lead.

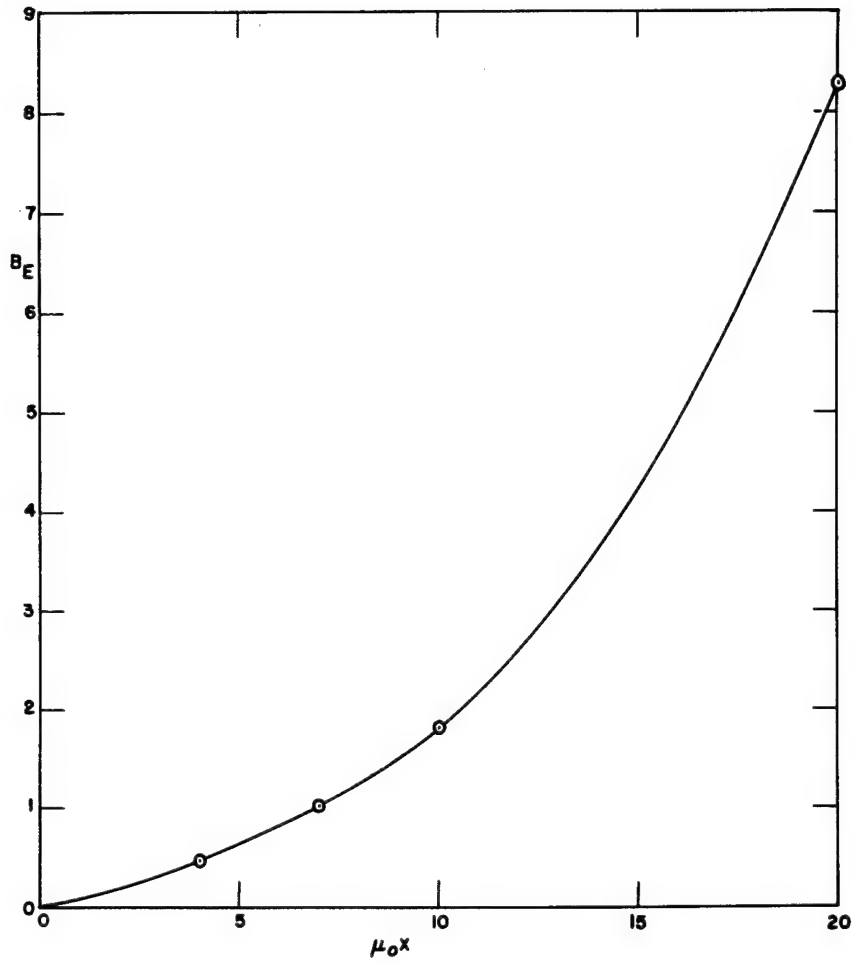

Figure C4 — Energy buildups vs. penetration; 7 Mev photons in lead.

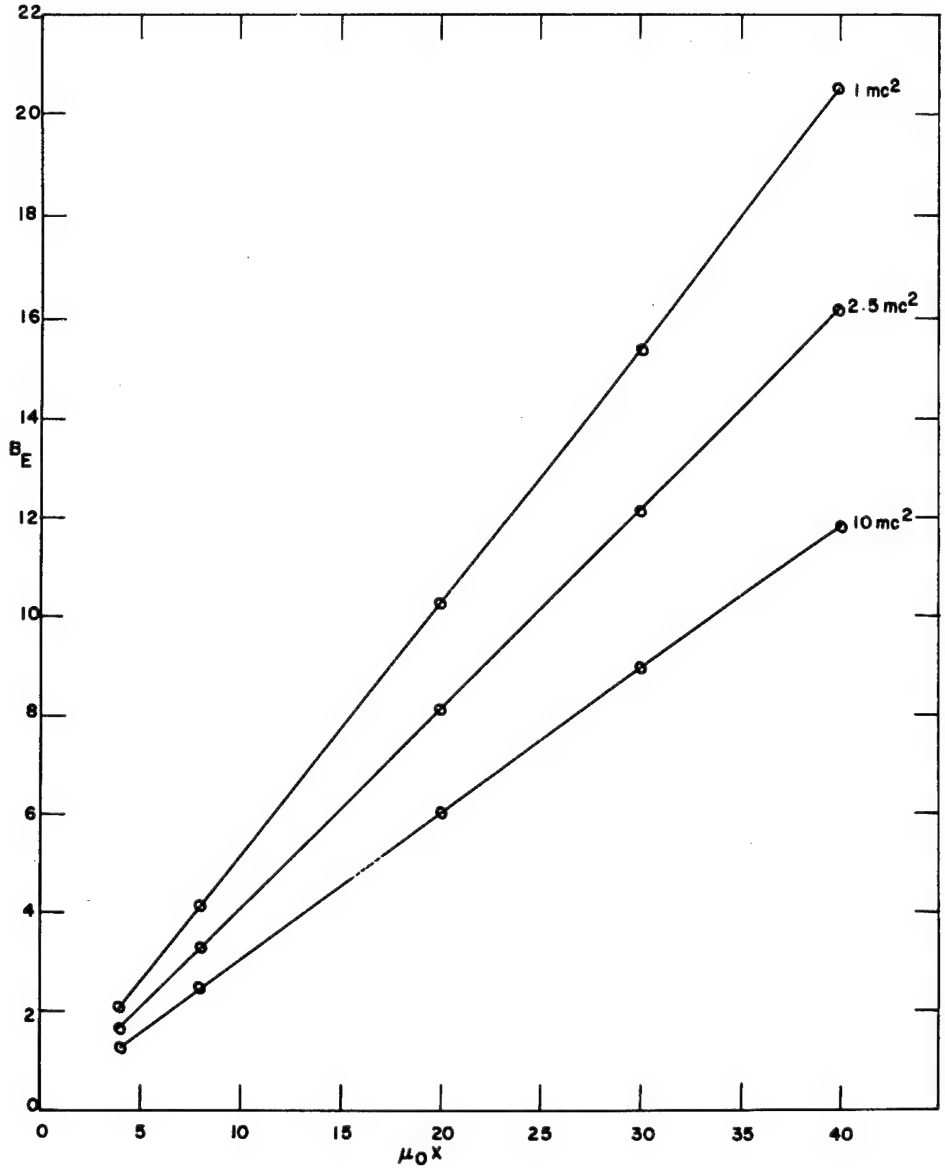

Figure C5 — Energy buildups vs. penetration; photons in pure Compton scatterer.

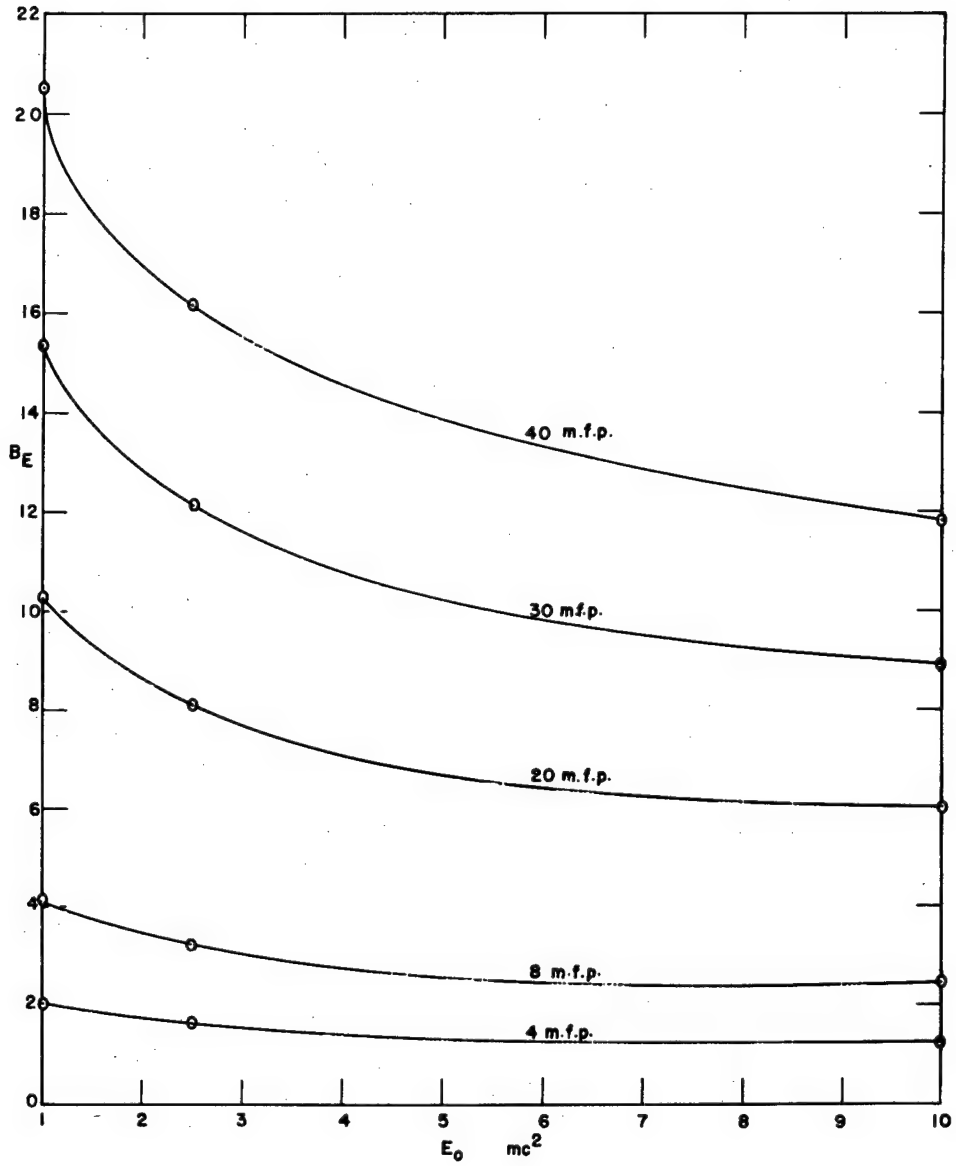

Figure C6 — Energy buildups vs. initial energy; photons in pure Compton scatterer.

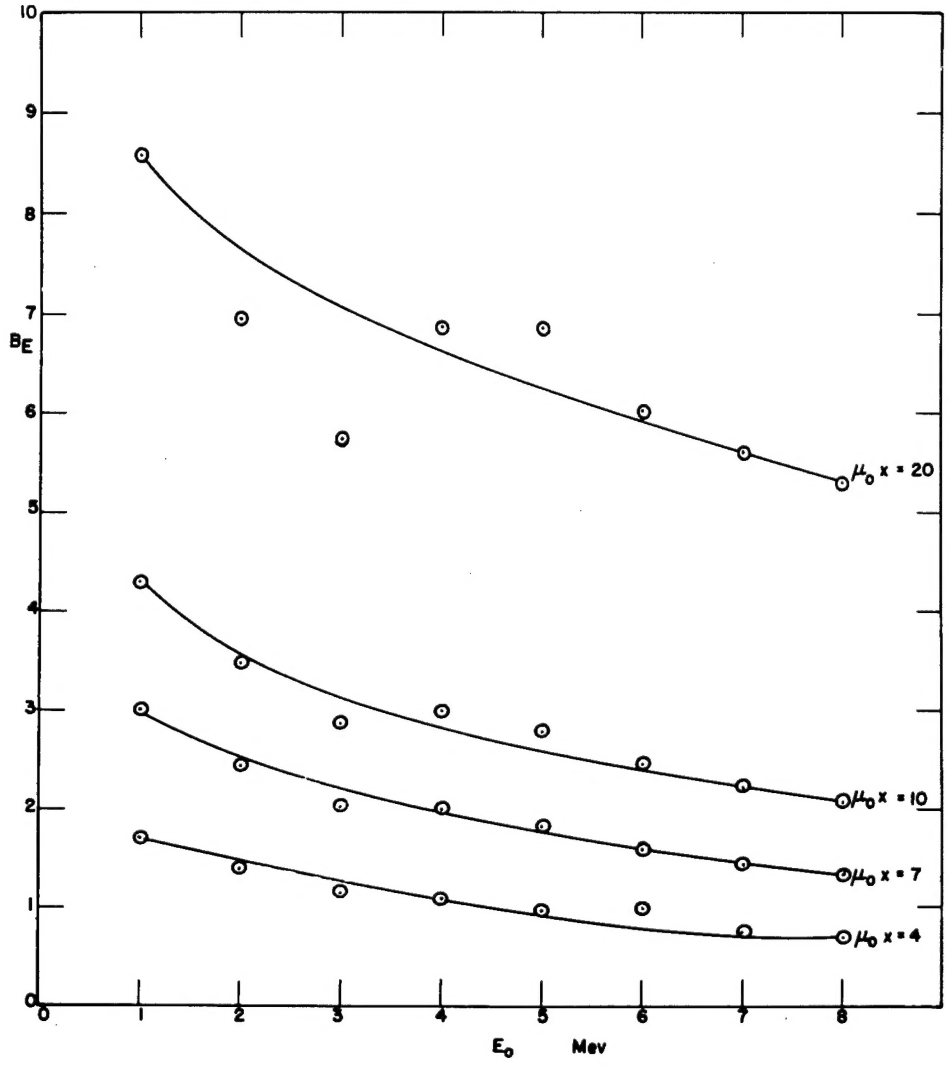

Figure C7 — Energy buildups vs. initial energy; photons in iron.

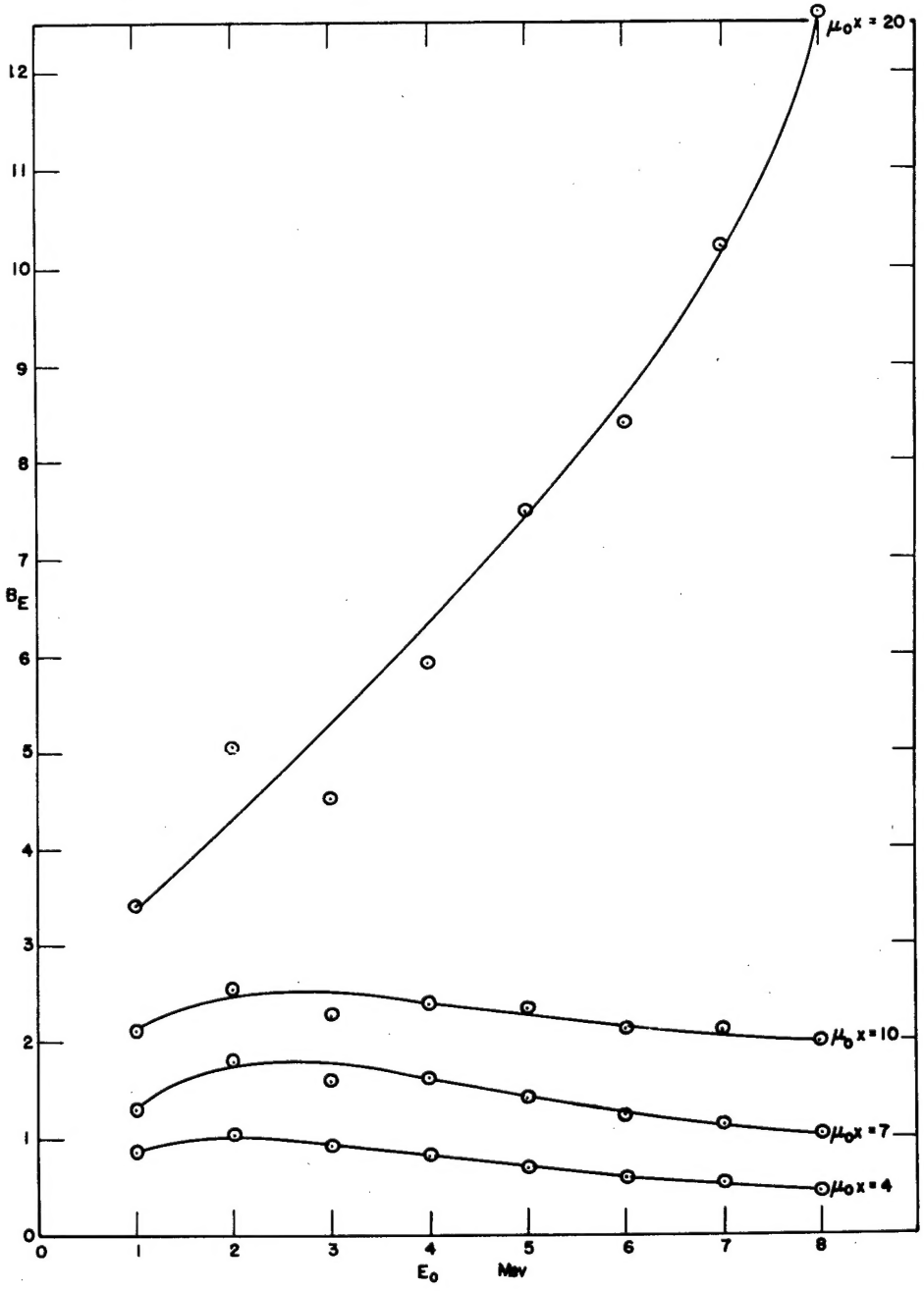

Figure C8 — Energy buildups vs. initial energy; photons in tungsten.

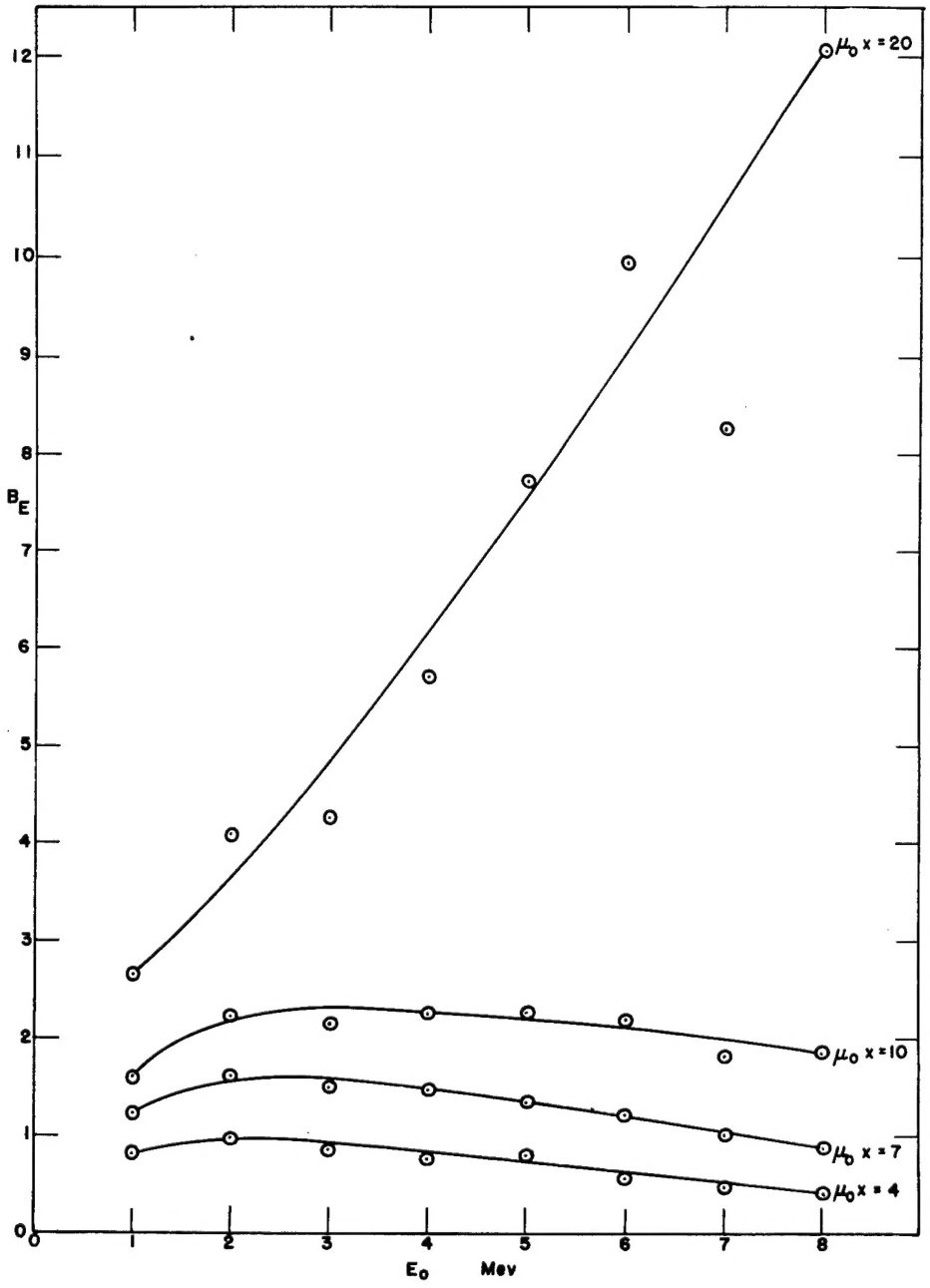

Figure C9 — Energy buildups vs. initial energy; photons in lead.

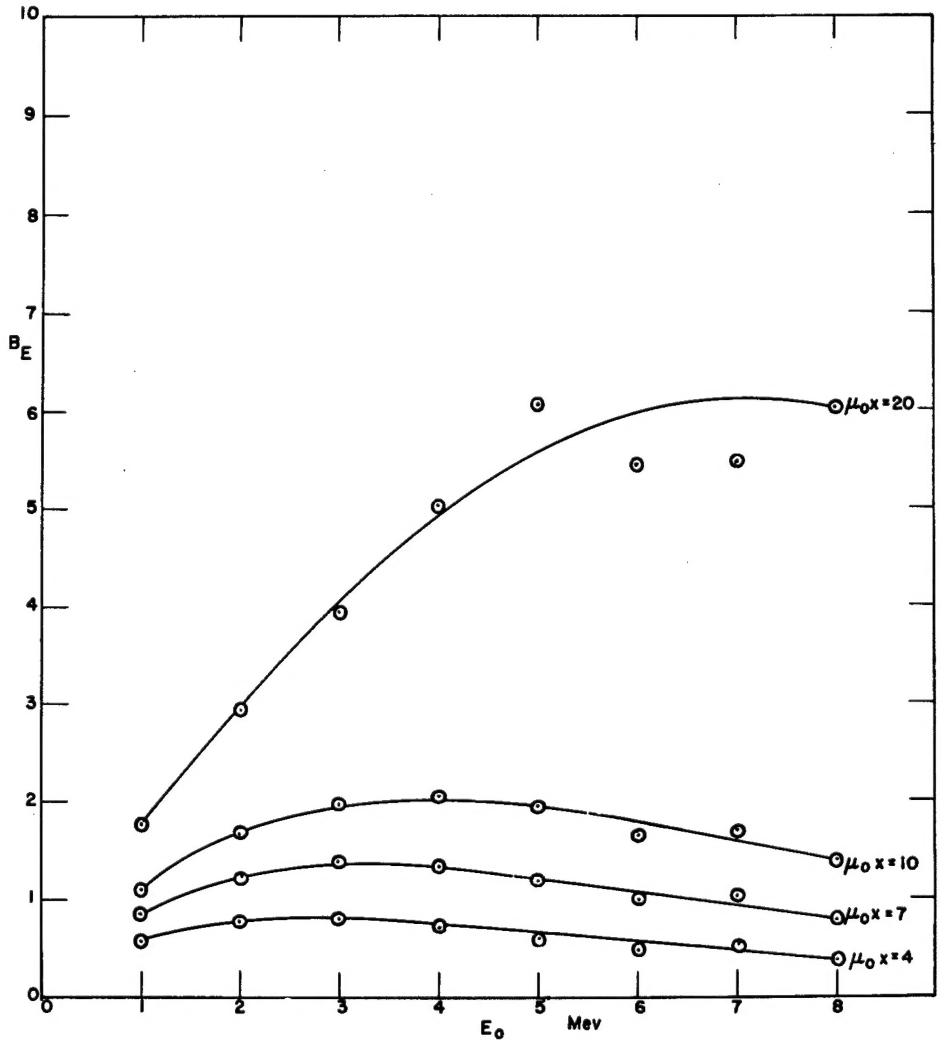

Figure C10 — Energy buildups vs. initial energy; photons in uranium.

END OF DOCUMENT